Hindawi
Mathematical Problems in Engineering
Volume 2020, Article ID 8820108, 24 pages
https://doi.org/10.1155/2020/8820108

Research Article

The Study of Optimization and Matching to Spring and Antiroll Bar Stiffness of Suspension for Multiresponse Target of Whole Vehicle under Sine-Swept Steering Input

Jin Gao and Fuquan Wu

Faculty of Transportation Engineering, Kunming University of Science and Technology, Kunming 650500, China

Correspondence should be addressed to Jin Gao; 906845822@qq.com

Received 18 September 2020; Revised 5 November 2020; Accepted 1 December 2020; Published 21 December 2020

Academic Editor: Dimitris Mourtzis

This article first leads from the specific double-wishbone suspension and multilink suspension structure form. And then systematically and detailedly analyse the change of spring's stiffness, and antiroll bar's stiffness causes the change of the side slip stiffness and rotation angle of tire, which will lead to the change of tire force, and then affect the dynamic characteristics of the whole vehicle. Based on this, the vehicle dynamics model considering the suspension is established, and the transfer function of the vehicle's response index to steering wheel angle with coupling spring stiffness and antiroll bar stiffness is derived. Based on the dynamic theory analysis of the suspension and the whole vehicle, the multibody dynamics model of the whole vehicle with front double-wishbone suspension and rear multilink suspension was established. By calculating the frequency response characteristics of the vehicle under the sine-swept input, the frequency response index at the normal steering wheel operating frequency of 0.5 Hz was obtained. In addition, these frequency response indexes at 0.5 Hz were taken as optimization objectives, and the spring stiffness and antiroll bar stiffness of the front and rear suspension were taken as optimization variables, which were optimized by the NSGA-II algorithm. The results show that at 0.5 Hz, the gain value in the frequency response index is reduced, and the delay time is not significantly different from other group schemes, but it is not the worst; the value is within an acceptable range, and the dynamic characteristics of the car in the low frequency range have been improved.

1. Introduction

The characteristic of suspension is very important to the vehicle's handling stability. The matching design of suspension's stiffness is one of the important methods to improve vehicle's handling stability. The matching of the suspension system's roll stiffness has direct influence on the handling stability and safety of the vehicle. For cars with independent suspension, the roll stiffness of the suspension is mainly composed of the spring's and the antiroll bar's stiffness.

Up to now, many experts and scholars have done a lot of research on the springs and antiroll bars of vehicle's suspension, so as to improve the vehicle's handling stability. Kazemi et al. studied the improvement of the operation handling stability of the whole vehicle whose front suspension is McPherson suspension and rear suspension is semitrailing arm suspension. A 9-DOF automotive dynamic model with McPherson suspension as the front suspension and semitrailing arm suspension as the rear suspension was established. After defining the offline optimization objective function and the online optimization objective function, the bee algorithm was used to optimize the vehicle's handling stability by optimizing the geometric parameters of the suspension. Finally, the comparison results show that the offline objective function optimization is better than the online objective function optimization. The handing stability has been improved [1]. Mastinu et al. proposed a formula to describe the dynamic of suspension based on the 1/4 vehicle model and gave the standard deviations of the analytical forms of vehicle's body acceleration, the relative displacement of sprung and unsprung mass, and the ground force,

respectively. The invariant points of the frequency response functions of active suspension and passive suspension are derived. The Pareto formula for selecting appropriate suspension parameters is given. The analytical formula they presented is useful to understand the suspension system [2–5]. Šagi et al. developed a new multiobjective optimization model to determine the optimal parameters of the suspension system. The new optimization model developed is to integrate a rapid simulation tool for suspension kinematics analysis and vehicle dynamics analysis with appropriate accuracy into a multiobjective optimization environment. On the basis of identifying the parameters that affect the suspension and defining the criteria for evaluating the dynamic characteristics of the vehicle, the multiobjective optimization of the suspension is carried out. Finally, the FMOGA-II algorithm is used to obtain the best results in terms of convergence, number of solutions, calculation time, and Pareto Frontier [6]. Javanshir et al. built a model based on dynamics software Trucksim, and the geometric parameters of the suspension system were optimized with antiroll bars and coil springs to improve ride comfort and handling stability of vehicles. The optimized vehicle is able to pass through the target direction with the minimum possible deviation, the minimum lateral acceleration, and minimal lateral slip [7]. Fossati et al. proposed an effective method to optimize the design of the vehicle's passive suspension system under random excitation and developed a numerical calculation program for vehicle state analysis. The objective function considers comfort and safety and combines with the NSGA-II algorithm for multiobjective optimization. The dynamic analysis results of the vehicle model are compared with the optimized and unoptimized suspension systems, and it is verified that the optimization can reduce the weighted RMS value of the vertical acceleration of the driver's seat by up to 21.14%, while improving the safety of the car [8]. Gobbi et al. proposed an optimization algorithm based on the local approximation of objective function and constraint function, and the suspension system of ground vehicle is optimized to achieve the optimal balance through grip, comfort, working space, and turning performance. Numerical results show that this algorithm has better precision and higher efficiency than some widely used optimization methods [9]. Gadhvi et al. use the most extensive multiobjective optimization algorithms NSGA-II, SPEA2, and PESA-II to optimize the passive suspension. The comparison results show that the Pareto Frontier of NSGA-II algorithm achieves an extreme trade-off advantage, and the optimal value of the target vector is slightly better than SPEA2 and PESA-II. SPEA2 and PESA-II were superior in maintaining Pareto optimal solution diversity [10, 11]. Shi et al. by parameterizing the geometric dimensions of the antiroll bar and optimizing the design of the antiroll bar for a certain car model, it is concluded that the antiroll bar with large lateral dip stiffness is helpful to improve the roll stability of the car [12].

The study of the above scholars improved the vehicle's handling stability from the suspension system, the stiffness of suspension's spring, and the antiroll bar. However, their researches are mainly based on the parameter-oriented model to improve the vehicle's handling stability and rarely involve the specific suspension structure form. Firstly, there is no in-depth discussion on the suspension characteristics of specific suspension structure and no in-depth explanation on the influence mechanism of spring and antiroll bar stiffness on suspension characteristics and vehicle's handling stability; it mainly includes three aspects: first, the above experts and scholars have not analyzed and clarified the relationship between the stiffness of spring and antiroll bar and the roll stiffness of suspension in detail; second, there is no detailed analysis of the roll center and instantaneous rotation center of the suspension, especially the analysis of instantaneous rotation center of the multilink suspension, which has a direct impact on the lateral load transfer; third, it did not analyze in detail the influence mechanism of suspension's roll stiffness and pitch stiffness on load transfer and the influence mechanism of load transfer on tire side slip stiffness, nor did it discuss in detail the influence mechanism of suspension's roll stiffness on wheel's toe angle and deformation angle. In addition, the above scholars did not propose an effective and feasible optimization matching method for the stiffness of spring and antiroll bar to make the vehicle's frequency characteristic indexes reach a better state for the specific suspension structure form.

For problems that experts have not solved, this article will be divided into four parts to write a statement of the research work done: the first part, first of all, the relationship between the stiffness of spring and the antiroll bar and the roll stiffness of the suspension is analyzed in detail, and then analysis the roll center and instantaneous rotation center of the suspension is analyzed in detail, especially the instantaneous rotation center of the multilink suspension. The second part will analyze in detail the influence mechanism of suspension's roll stiffness on tire's side slip stiffness from the angle of lateral and longitudinal load transfer, and the influence mechanism of suspension roll stiffness and pitch stiffness on toe angle, deformation angle, camber angle, and vehicle's lateral dynamics. In the third part, on the basis of the analysis in the previous two parts, the total lateral force generated by suspension on the tire was mainly described. After ignoring some factors, the multibody dynamic model of the whole vehicle with the front double-wishbone suspension and rear multilink suspension coupling spring stiffness and antiroll bar stiffness was established. In the fourth part, the spring stiffness and antiroll bar stiffness of the front and rear suspension are taken as optimization variables, and the frequency response indexes corresponding to 0.5 Hz of the whole vehicle under the of sine-swept input are taken as optimization target for multiobjective optimization, so as to carry out matching design for the suspension spring stiffness and antiroll bar stiffness. Finally, Pareto solution set and relative optimal solution of frequency response indexes under sine-swept input are obtained. The relative optimal solution is compared with the original vehicle's simulation data to verify whether the frequency response performance of the car has been improved.

2. Analysis of the Force of Suspension's Spring and the Antiroll Bar

The stiffness of the suspension's spring and the antiroll bar has important effect on the roll characteristic of the vehicle. And it greatly affects and determines the roll stiffness of the suspension. The installation of coil spring and the force of suspension are shown in Figure 1 [13].

In Figure 1, F is the support force of the suspension from the ground; F_L is the force on the suspension's transverse arm from the vehicle's body; F' is the force on the shock absorber from the vehicle's body; and F' can be decomposed into the force F_F that acts on the axis of shock absorber and the force F_Q that acts on the axis that perpendicular to the axis of shock absorber. The force F_F acting on the shock absorber's axle is supported by the shock absorber's spring, and the force F_Q acting on the axle that perpendicular to the shock absorber's axle is borne by the shock absorber's upper end. η is the angle between the force F' that acts on the shock absorber and the shock absorber's axle.

The force of the antiroll bar is shown in Figure 2. When the vertical displacement of the right and left wheel is different, the antiroll bar will produce a torsional stiffness $K_{\varphi w}$. And then the rolling force F_A that acts on the end of the antiroll bar will be produced.

According to the force diagram of the antiroll bar, in the moment of the car's rolling, the torque acting on the sprung mass and unsprung mass is

$$M_{\mathrm{AR}} = K_{\varphi w}\frac{l_c l_0}{l_e^2}\cdot\phi - K_{\varphi w}\frac{l_c^2}{l_e^2}\cdot\phi_u, \tag{1}$$

where l_c is the length of the antiroll bar's straight rod part; l_0 is the distance between the two rubber bushes; and l_e is the vertical displacement between the antiroll bar's endpoint and the straight rod part. ϕ is the roll angle of sprung mass; ϕ_u is the roll angle of unspung mass.

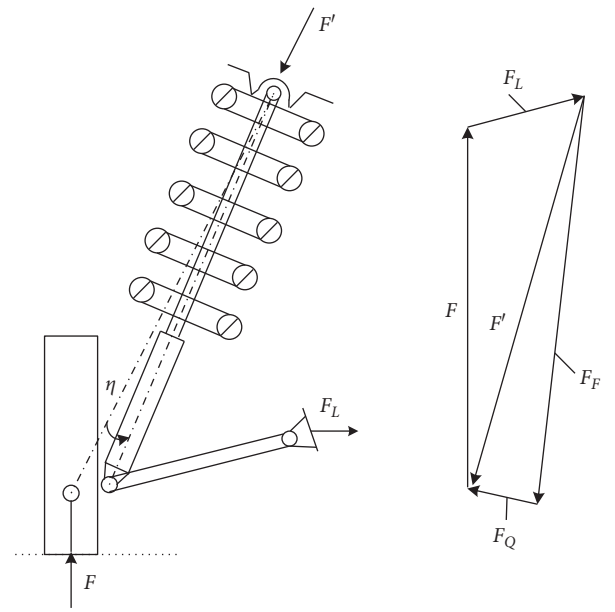

Figure 1: The installation of coil spring and the force of suspension.

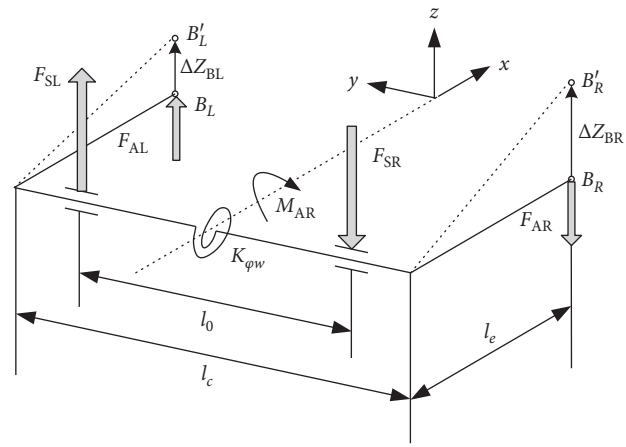

Figure 2: The force diagram of the car's antiroll bar.

3. Analysis of Suspension's Roll Stiffness and Roll Center

The roll stiffness and roll center are important parameters of suspension which can affect the loading transfer between left and right wheels and make tire's side slip stiffness change in the course of the vehicle's motion. For the vehicle in this paper, the front suspension is a double-wishbone suspension and the rear suspension is multilink suspension.

3.1. Roll Stiffness Analysis of the Suspension. The total roll stiffness of the car is mainly composed of the roll stiffness of the front suspension and the rear suspension, that is,

$$K_\phi = K_{\phi f} + K_{\phi r}, \tag{2}$$

where K_ϕ is the total roll stiffness of the car; $K_{\phi f}$ is the roll stiffness of the front suspension; and $K_{\phi r}$ is the roll stiffness of the rear suspension. The roll stiffness of front suspension and rear suspension are combined with the stiffness that the spring contributed and the stiffness that the antiroll bar contributed, that is,

$$K_{\phi f} = K_{\phi fs} + K_{\phi fw}, \tag{3}$$

$$K_{\phi r} = K_{\phi rs} + K_{\phi rw}, \tag{4}$$

where $K_{\phi fs}$ and $K_{\phi rs}$ are the roll stiffness that the front and rear suspension's spring contributed, respectively, and $K_{\varphi fw}$ and $K_{\phi rw}$ are the roll stiffness that the front and rear suspension's antiroll bar contributed, respectively.

Figure 3 shows the mechanical model where the spring stiffness of the double-wishbone independent suspension contributes to the roll stiffness of the suspension. The sprung mass is fixed, and the ground rotates an angle Φ around the intersection E of the car's center line and the ground.

It can be obtained from Figure 3 that the roll stiffness is

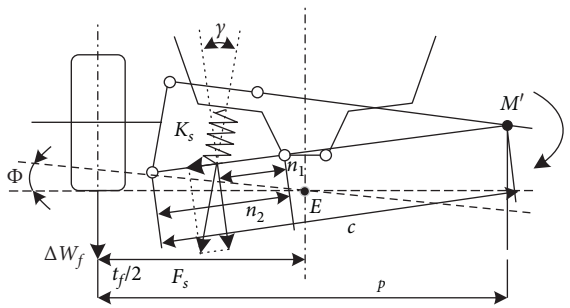

Figure 3: The dynamic model of double-wishbone suspension's roll stiffness.

$$K_{\phi f} = \frac{dT}{d\Phi} = \frac{1}{2} \cdot K_s \cdot \left(\frac{c \cdot n_1 \cdot t_f}{p \cdot n_2} \cdot \cos\gamma \right)^2, \tag{5}$$

where T is the torque that the ground acts on the suspension to prevent it from rotating. ΔW_f is the increment of the force of the wheel to the ground. t_f is the front wheel center distance. K_s is the spring's linear stiffness. γ is the intersection angle. The point M' is the instantaneous rotation center. p,, c, n_1, and n_2 are the lever's length.

In order to analysis the roll stiffness and the change of the roll center of double-wishbone suspension and multilink suspension during the driving of the car. Dynamic models of the car's front double-wishbone suspension and rear multilink suspension shown in Figures 4 and 5 are built in ADAMS/CAR software [14].

Figures 6 and 7 show the influence trend of antiroll bar's stiffness and spring's stiffness on the suspension's roll stiffness. In Figure 6, the front and rear suspensions increase in a nonlinear manner as the stiffness of the antiroll bar increases. When the antiroll bar stiffness gradually increases in the range of 40 N/m and 60 N/m, the roll stiffness of the front suspension and rear suspension increases slowly. When the antiroll bar stiffness increases to 60 N/m, the roll stiffness of the front suspension and rear suspension will increase at a large rate as the stiffness of the antiroll bar increases. In Figure 7, the roll stiffness of front suspension and rear suspension increases linearly with the increase of spring stiffness of front and rear suspensions.

3.2. Analysis of the Multilink Suspension's Roll Center. Figure 8 shows the solid model of multilink suspension. The motion of the multilink suspension is complicated. In order to find the multilink suspension's instantaneous rotation axis, some necessary simplifications are needed [15].

Figure 9 shows a schematic diagram after equivalent transformation of the actual multilink suspension. Plane a is determined through three points ①, ③, and ② of the lower suspension arm. The extension line of extroverted arm ④ and ⑤ intersects plane a at point A. Making the plane d perpendicular to extroverted arm through point (5), the axle 1 can be obtained through points ① and ②, and the axle 2 can be obtained through points ③ and ⑧. V_3 and V_8 can be obtained as point ③, and point ⑧ rotates around axle 1. It is easy to get $V_{(5)3}$ as point (5) exercises relative to point ③.

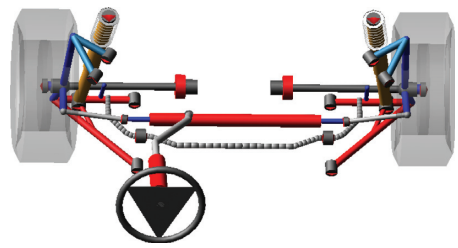

Figure 4: The dynamic model of vehicle's double-wishbone suspension.

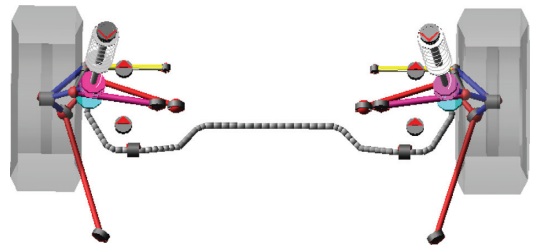

Figure 5: The dynamic model of vehicle's multilink suspension.

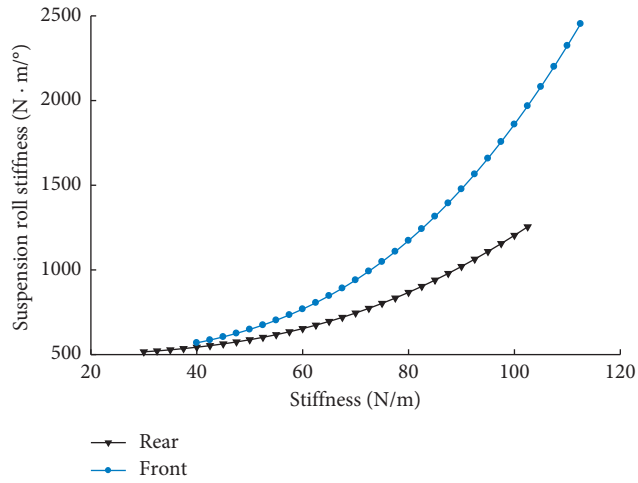

Figure 6: The influence trend of antiroll bar's stiffness on suspension's roll stiffness.

Make the plane e that parallel to V_3 through point (5) and point $V_{(5)3}$. The alternating line of plane d and plane e is the motion direction of point (5) shown as $V_{(5)}$. Make plane f perpendicular to $V_{(5)}$ through point (5). The alternating line of plane f and plane a is the instantaneous roll axle during multilink suspension's motion.

The instantaneous axis of rotation of the suspension intersects the cross section through the axle of the car at a point, which is the instantaneous center of rotation. The point where the connection line between the instantaneous rotation center and the bottom of the suspension's tire intersects the longitudinal section of the car is the roll center. As shown in Figure 10, it is the change of the roll center's height of the suspension with the tire jumping. In Figure 10, the roll center's height of the rear suspension is higher than that of the front suspension, and the difference of the roll

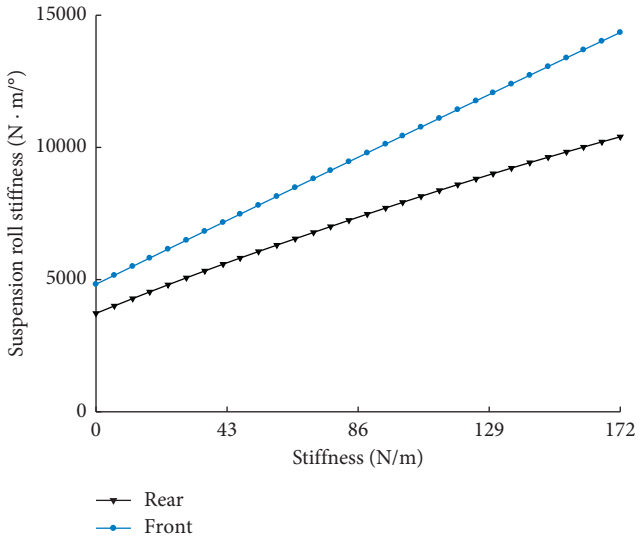

Figure 7: The influence trend of spring's stiffness on suspension's roll stiffness.

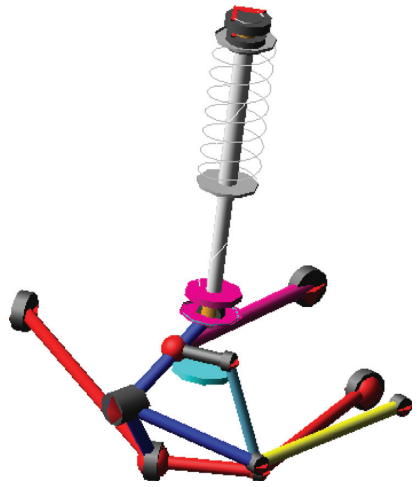

Figure 8: The solid model of multilink suspension.

center's height of the front and rear suspensions becomes larger and larger as the wheel is jumping.

4. Analysis of Lateral and Longitudinal Load Transfer during Vehicle's Motion

Car's body will roll when the car turns and changes line, and the roll angle should be controlled in a reasonable range in car's movement. Therefore, it is necessary to design reasonable suspension's roll stiffness. The rolling of the car's body is shown in Figure 11. Figure 12 shows the rolling model of the front axle of the car, and this model is obtained by the simplification of the front suspension of this paper.

In Figure 11, m_s is the sprung mass. m_u is the unsprung mass. A_j is the lateral acceleration of sprung mass. a_y is the lateral acceleration of unsprung mass. h_s is the distance between the mass center of sprung mass and the roll center o_s. h_0^* is the distance between the suspension's roll center and the road surface. r is the wheel's radius. ϕ is the roll angle of the vehicle's body. The torque caused by the suspension centrifugal force is $M_1 = m_s A_j h_s$. The roll torque caused by the mass gravity of the sprung mass is $M_2 = m_s g h_s \phi$. For independent suspension, the roll torque caused by the centrifugal force of unspung mass is $M_3 = -m_u a_y (h_0^* - r)$.

In Figure 11, according to the torque equilibrium condition, the following can be obtained:

$$K_\phi \phi = m_s A_j h_s + m_s g h_s \phi - m_u a_y (h_0^* - r). \tag{6}$$

According to equation (6), the total roll stiffness and steady-state roll angle of the suspension can be obtained as follows:

$$K_\phi = \frac{m_s A_j h_s + m_u a_y (h_0^* - r)}{\phi} + m_s g h, \tag{7}$$

$$\phi = \frac{m_s A_j h_s - m_u a_y (h_0^* - r)}{K_{\phi f} + K_{\phi r} - m_s g h_s}. \tag{8}$$

For the simplified suspension model shown in Figure 12, the transformation between the linear stiffness and angular stiffness of the front and rear suspension's spring is

$$K_{\phi fs} = \frac{1}{2} K_{fs} \left(\frac{t_f l_{2f}}{l_{1f}} \right)^2, \tag{9}$$

$$K_{\phi rs} = \frac{1}{2} K_{rs} \left(\frac{t_r l_{2r}}{l_{1r}} \right)^2, \tag{10}$$

where K_{fs} and K_{rs} are the linear stiffness of the front and rear suspension's springs, respectively. l_{1f} is the length of the fore arm. l_{1r} is the length of the rear arm. l_{2f} is the distance between the spring's installation position of the front suspension and the hinge point of the arm. l_{2r} is the distance between the spring's installation position of the rear suspension and the hinge point of the arm. t_f and t_r are the wheel center distance of the front and rear suspension, respectively.

Substituting equations (3) and (4) into equation (2), the total roll stiffness K_ϕ of vehicle can be obtained:

$$K_\phi = K_{\phi f} + K_{\phi r} = K_{\phi fs} + K_{\phi fw} + K_{\phi rs} + K_{\phi rw}. \tag{11}$$

For the inertial forces acting on the vehicle, there must be an equilibrium tire force. The inertial force acting on the center of mass decomposes to the front and rear wheels:

$$\frac{(m_s A_j + m_u a_y) a}{(a + b)}, \tag{12}$$

$$\frac{(m_s A_j + m_u a_y) b}{(a + b)}, \tag{13}$$

where a is the distance from the vehicle's center of mass to the front axle. b is the distance from the vehicle's center of mass to the rear axle.

If the vehicle's body rolls, load transfer will occur between the left and right wheels of the front and rear axles. Let

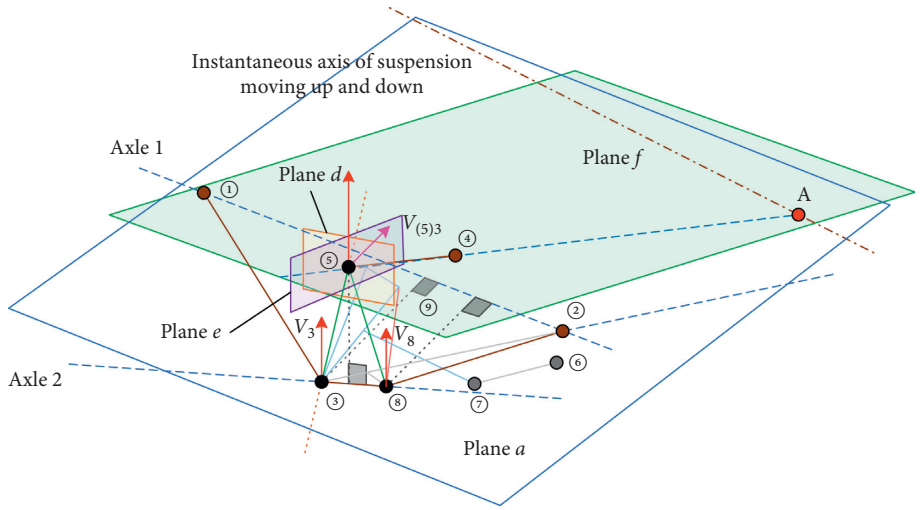

Figure 9: Schematic diagram of the instantaneous roll axle of the multilink suspension.

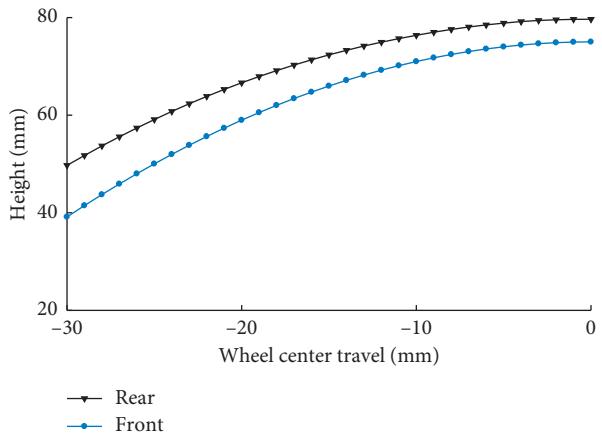

Figure 10: The change of the roll center's height of the suspension with the tire jumping.

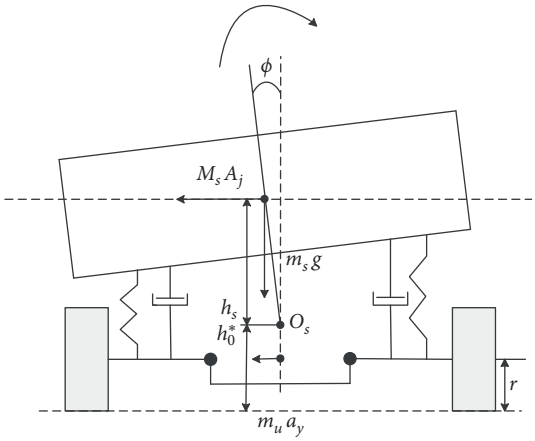

Figure 11: Vehicle's rolling model.

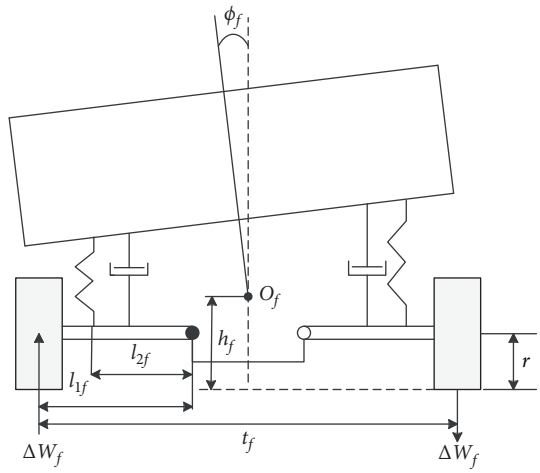

Figure 12: Vehicle's front axle's rolling model.

the load transfer quantities of the front axle and rear axle of the vehicle be ΔW_f and ΔW_r, respectively. In the plane of the front and rear wheels perpendicular to the longitudinal direction of the vehicle, it can be obtained from the torque balance around the corresponding roll center:

$$K_{\phi f}\phi = \Delta W_f t_f - \frac{\left(m_s A_j + m_u a_y\right)b}{(a+b)} h_f, \tag{14}$$

$$K_{\phi r}\phi = \Delta W_r t_f - \frac{\left(m_s A_j + m_u a_y\right)a}{(a+b)} h_r. \tag{15}$$

Substitute equation (8) into equations (14) and (15), ΔW_f and ΔW_r can be obtained as follows:

$$\Delta W_f = \frac{K_{\phi f}}{t_f}\left[\frac{m_s A_j h_s - m_u a_y\left(h_{of}^* - r\right)}{K_{\phi f} + K_{\phi r} - m_s g h_s} + \frac{\left(m_s A_j + m_u a_y\right)b}{a+b} h_f\right], \tag{16}$$

$$\Delta W_r = \frac{K_{\phi r}}{t_r}\left[\frac{m_s A_j h_s - m_u a_y\left(h_{or}^* - r\right)}{K_{\phi f} + K_{\phi r} - m_s g h_s} + \frac{\left(m_s A_j + m_u a_y\right)a}{a+b} h_r\right]. \tag{17}$$

The load transfer of the car not only occurs between the left and right wheels but also happens between the front and rear axles of the car. When the car is accelerating or braking, load transfer will occur between the front and rear axles. The load transfer between the front and rear axles of the vehicle is

$$\Delta W = \frac{h\left(m_s + m_u\right)\ddot{x}}{a+b}, \tag{18}$$

where h is the distance between the vehicle's center of mass and the ground, $h = h_s + h_0^*$.

5. Effect of Load Transfer and Longitudinal Force on Tire's Side Slip Stiffness

If the vehicle's body rolls, load transfer will occur between the left and right wheels. When the car's body pitches, the load transfer will occur between the front and rear axles. The tire's side slip stiffness will be affected when the load transfer occurs, and vehicle's handling stability will be affected too.

5.1. Change of Tire's Side Slip Stiffness While Only considering Load Transfer between Left and Right Wheels. According to the analysis in the above part, it is known that load transfer will occur between the left and right wheels when the vehicle is rolling, and the load transfer will cause the change of the tires' side slip stiffness. Taking the front axle as an example, when no lateral force is applied to the vehicle, the vertical load of the left and right wheels of the axle is W_{f0}, and the side slip stiffness of each tire is K_{f0}. When there is lateral force acting on the car and the ground, there is a corresponding reaction force F_{fy} acting on the front axle's two tires. If the vertical load of the left and right wheels does not change, the corresponding side slip angle is

$$\lambda_{f0} = \frac{F_{fy}}{2K_{f0}}. \tag{19}$$

In fact, the vertical load of the left and right wheels will change when the lateral force acts on the vehicle. The inside wheel reduces ΔW_f, and the outboard wheel increases ΔW_f; the side slip stiffness of the two tires then becomes K_{f1} and K_{f2}. Due to left and right tire's side slip angle is equal,

$$F_{fy} = K_{f1}\lambda_f + K_{f2}\lambda_f. \tag{20}$$

Make $K_{f0}' = (K_{f1} + K_{f2})/2$, where K_{f0}' is the average side slip stiffness of each tire after vertical load redistribution, so the side slip angle of the left and right wheels is

$$\lambda_f = \frac{F_{fy}}{2K_{f0}'}. \tag{21}$$

Due to the change curve of the side slip stiffness of the left and right tires is a smooth curve protruding upward, from the geometrical point of view, $K_{f0} > K_{f0}'$ and $\lambda_f > \lambda_{f0}$. Further analysis shows that the greater the vertical load difference between the left and right wheels, the smaller the average side slip stiffness. The side slip stiffness of the rear tires is the same as the front tires.

Thus, under the action of lateral force, if the vertical load of the front axle's left and right wheels of the car changes greatly, cars tend to increase understeer. If the vertical load of the left and right wheels of the rear axle changes greatly, the car tends to reduce the understeer. The load variation of the left and right wheels of the front and rear axles of a car is determined by a series of parameters such as the roll stiffness of the front and rear suspensions, the sprung mass, the unspung mass, the center of mass' position, and the roll center of the front and rear suspensions.

5.2. Tires' Side Slip Stiffness While considering Longitudinal Load Transfer and Longitudinal Forces. The previous analysis is based on the conclusion that longitudinal load transfer and longitudinal force are ignored. However, there is a longitudinal load transfer during the actual motion of the car. If the influence of load transfer on roll stiffness is small, it can be regarded as the first order. If the driving/braking force is a small relative to the tire load, the side slip stiffness of the tire can be simulated by a simple parabolic function. For small longitudinal and lateral accelerations,

$$\frac{\partial K_f}{\partial W}\frac{\Delta W_f}{K_{f0}}, \quad \frac{\partial K_f}{\partial W}\frac{\Delta W}{K_{f0}}, \quad \left(\frac{2X_f}{\mu W_f}\right)^2. \tag{22}$$

They are treated as tiny quantities of the same order of magnitude. Based on these simplifications, the side slip

stiffness can be expressed by the following formula at a small side slip angle:

$$\begin{cases} K_{f1} = K_{f0}\left[1 - \dfrac{\partial K_f}{\partial W}\dfrac{\Delta W_f}{K_{f0}} - \dfrac{\partial K_f}{\partial W}\dfrac{\Delta W}{2K_{f0}} - \dfrac{1}{2}\left(\dfrac{2X_f}{\mu W_f}\right)^2\right], \\ K_{f2} = K_{f0}\left[1 + \dfrac{\partial K_f}{\partial W}\dfrac{\Delta W_f}{K_{f0}} - \dfrac{\partial K_f}{\partial W}\dfrac{\Delta W}{2K_{f0}} - \dfrac{1}{2}\left(\dfrac{2X_f}{\mu W_f}\right)^2\right], \\ K_{r1} = K_{r0}\left[1 - \dfrac{\partial K_r}{\partial W}\dfrac{\Delta W_r}{K_{r0}} - \dfrac{\partial K_r}{\partial W}\dfrac{\Delta W}{2K_{r0}} - \dfrac{1}{2}\left(\dfrac{2X_r}{\mu W_r}\right)^2\right], \\ K_{r2} = K_{r0}\left[1 + \dfrac{\partial K_r}{\partial W}\dfrac{\Delta W_r}{K_{r0}} - \dfrac{\partial K_r}{\partial W}\dfrac{\Delta W}{2K_{r0}} - \dfrac{1}{2}\left(\dfrac{2X_r}{\mu W_r}\right)^2\right], \end{cases} \tag{23}$$

where W is the mass of the car, $W = m_s + m_u$. ΔW_f is the load transfer amount between the left and right wheels of the front axle when the car turns. ΔW is the amount of load transfer between the front and rear axles caused by the driving force or braking force, and W_f is the vertical load of the front axle $W_f = bW/(a+b)$. μ is the coefficient of friction between the tire and the road. X_f and X_r are the longitudinal force on the front and rear tires of the vehicle; $X_f = \alpha_c W\ddot{x}/2$, and $X_r = (1-\alpha_c)W\ddot{x}/2$. α_c is the distribution coefficient of driving force or braking force. l is the wheelbase of the car, $l = a + b$. $\ddot{x}$ is the longitudinal acceleration caused by driving force or braking force. h is the height between the vehicle's center of mass and the ground. ΔW_r is the load transfer amount of the left and right wheels of the rear axle. W_r is the vertical load of the rear axle, $W_r = aW/(a+b)$.

From the above analysis, it can be known that the equivalent lateral stiffness of the front and rear axles can be obtained by superposing the lateral stiffness of the left and right tires, respectively. If $\ddot{x}$ is used to represent the equivalent side slip stiffness of the front and rear axles of the car, then

$$\begin{cases} 2K_f^* \approx 2K_{f0}\left[1 + \dfrac{hW}{2lK_{f0}}\dfrac{\partial K_f}{\partial W}\ddot{x} + \dfrac{1}{2}\left(\dfrac{\alpha_c l}{ub}\right)^2\ddot{x}^2\right], \\ 2K_r^* \approx 2K_{r0}\left[1 - \dfrac{hW}{2lK_{r0}}\dfrac{\partial K_f}{\partial W}\ddot{x} + \dfrac{1}{2}\left(\dfrac{(1-\alpha_c)l}{ua}\right)^2\ddot{x}^2\right]. \end{cases} \tag{24}$$

6. Change of Wheels' Toe Angle and Deformation Steering Angle

If the vehicle has longitudinal acceleration $\ddot{x}$ and lateral acceleration $\ddot{y}$ at meantime, the body will have pitch and roll motion. This will cause the suspension's stroke to change, resulting in the change of the toe angle and the deformation steering angle.

6.1. Change of Wheels' Toe Angle. Suppose the vehicle's pitch and roll axes are on the ground, and the toe angle's change of the front wheel caused by the pitching motion is $(\partial\alpha_f/\partial z)(ahW\ddot{x}/K_\theta)$. Similarly, the toe angle's change caused by the roll motion is $(\partial\alpha_f/\partial z)(t_f hW\ddot{y}/2K_\phi)$. $\partial\alpha_f/\partial z$ is the toe angle's change in the unit suspension's stroke. K_θ is the pitch stiffness. K_ϕ is the roll stiffness.

Figure 13 shows the curve of the front and rear suspension's toe angle with the wheel's displacement when the wheels' bouncing in the reverse direction [16].

In Figure 13, during the downward bouncing of the wheels, the toe angle of the front suspension wheels (the inner wheel when turning) increases in the positive direction, and the toe angle of the rear suspension wheels (the inner wheel when turning) increases in the negative direction. The toe angle of the corresponding outer wheels of the front suspension increases negatively, and the toe angle of the outer wheels of the rear suspension increases positively. For the front suspension, the toe angle of the inner wheels increases positively, and the toe angle of the outer wheels increases negatively, which will increase the understeer characteristics of the car. For the rear suspension, the toe angle of the inner wheel increases negatively, and the toe angle of the outer wheel increases positively, which will also increase the understeer characteristics of the car.

6.2. Change of Wheels' Deformation Steering Angle. In addition to of the toe angle' change, the torque T_s applied to the steering system due to the tire's lateral force $2F_y = b/lW\ddot{y}$ and longitudinal force $X_f = \alpha_c W\ddot{y}$ acting on the front wheels will cause deformation steering angle to change, where T_s is

$$T_s = 2\xi F_y + \frac{F_y}{K_y}2X_f = \left(\xi + \frac{\alpha_c W}{2K_y}\ddot{x}\right)\frac{bW}{l}\ddot{y}, \tag{25}$$

where K_y is the side slip stiffness of the tire. ξ is the sum of the tire drag and the rearward drag of the kingpin. For each wheel, the sum of the toe angle's change, and the deformation steering angle can be expressed as follows:

$$\begin{aligned} \alpha_{f1} = {} & \frac{\partial\alpha_f}{\partial z}\frac{ahW}{K_\theta}\ddot{x} + \frac{\partial\alpha_f}{\partial z}\frac{t_f hW}{2K_\phi}\ddot{y} - \frac{\partial\alpha_f}{\partial X}\frac{\alpha_c W}{2}\ddot{x} \\ & - \frac{\partial\alpha_f}{\partial T}\left(\xi + \frac{\alpha_c W}{2K_y}\ddot{x}\right)\frac{bW}{l}\ddot{y}, \end{aligned} \tag{26}$$

$$\begin{aligned} \alpha_{f2} = {} & -\frac{\partial\alpha_f}{\partial z}\frac{ahW}{K_\theta}\ddot{x} + \frac{\partial\alpha_f}{\partial z}\frac{t_f hW}{2K_\phi}\ddot{y} - \frac{\partial\alpha_f}{\partial X}\frac{\alpha_c W}{2}\ddot{x} \\ & - \frac{\partial\alpha_f}{\partial T}\left(\xi + \frac{\alpha_c W}{2K_y}\ddot{x}\right)\frac{bW}{l}\ddot{y}, \end{aligned} \tag{27}$$

$$\alpha_{r1} = -\frac{\partial\alpha_r}{\partial z}\frac{ahW}{K_\theta}\ddot{x} + \frac{\partial\alpha_r}{\partial z}\frac{t_r hW}{2K_\phi}\ddot{y} - \frac{\partial\alpha_r}{\partial X}\frac{(1-\alpha_c)W}{2}\ddot{x}, \tag{28}$$

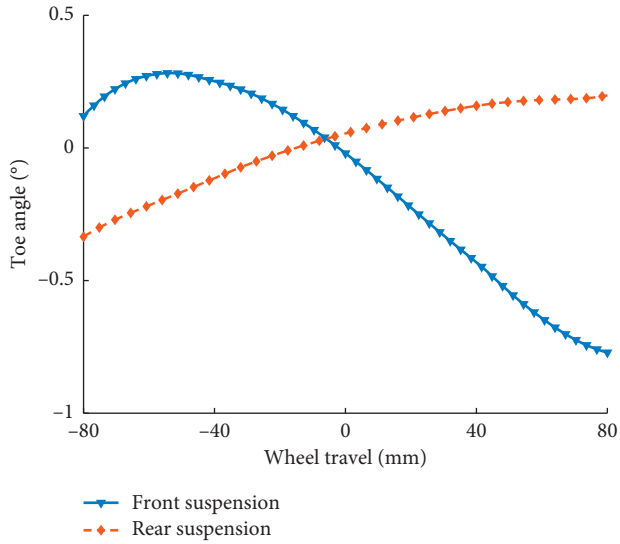

Figure 13: The curve of the toe angle of the front and rear wheels with the wheel's displacement.

$$\alpha_{r2} = \frac{\partial \alpha_r}{\partial z}\frac{bhW}{K_\theta}\ddot{x} + \frac{\partial \alpha_r}{\partial z}\frac{t_r hW}{2K_\phi}\ddot{y} - \frac{\partial \alpha_r}{\partial X}\frac{(1-\alpha_c)W}{2}\ddot{x}, \quad (29)$$

where $\partial\alpha_f/\partial X$ and $\partial\alpha_r/\partial X$ are the deformation steering angles of the unit longitudinal force of the front and rear suspension systems, respectively. $\partial\alpha_f/\partial X$ is the deformation steering angle of the unit steering torque.

Figure 14 shows the change of vehicle's toe angle with longitudinal force. In Figure 14, when the longitudinal force is positive, it is the driving force, and when the longitudinal force is negative, it is the braking force. As the braking force increases, the toe angle of the front suspension increases in the negative direction, and the toe angle of the rear suspension increases in the positive direction. As the driving force increases, the toe angle of the front suspension increases positively, and the toe angle of the rear suspension increases negatively.

Figure 15 shows the curve of the front and rear suspensions' toe angle with the aligning torque. In Figure 15, as the wheel's aligning force increases, the toe angle of the front suspension and the rear suspension decreases correspondingly.

7. Lateral Force of the Car's Tires Generated by Suspension

For vehicles in motion, the front and rear wheels are subjected to lateral forces resulting from the deformation of the tire. As mentioned earlier, the suspension can cause changes in the side slip stiffness and steering angle of the tire, which can change the tire force.

The roll of the body will cause the wheel's camber angle to change. The camber angle of the wheel will produce lateral force acting on the tire. At the same time, for a moving vehicle, the front and rear wheels are subjected to lateral forces caused by tire deformation. Taking into account the

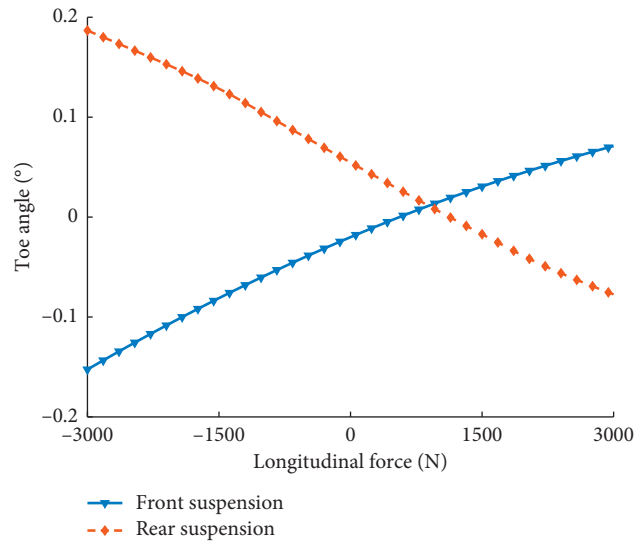

Figure 14: The curve of vehicle's toe angle with longitudinal force.

roll of the vehicle body, the force F_{y1} caused by suspension that acts on the side of the tires is expressed as follows:

$$F_{y1} = Y_{f1} + Y_{f2} + Y_{r1} + Y_{r2} + 2Y_{cf} + 2Y_{cr}, \quad (30)$$

$$\begin{cases} 2Y_{cf} = -2Z_{cf}\dfrac{\partial \sigma_f}{\partial \phi}\phi, \\ 2Y_{cr} = -2Z_{cr}\dfrac{\partial \sigma_r}{\partial \phi}\phi, \end{cases} \quad (31)$$

where Y_{f1}, Y_{f2}, Y_{r1}, and Y_{r2} are the lateral force caused by the deformation of the vehicle's tires. Y_{cf} and Y_{cr} are the lateral camber thrust on the front and rear tires of the car. Z_{cf} and Z_{cr} are the lateral camber thrust coefficients of the

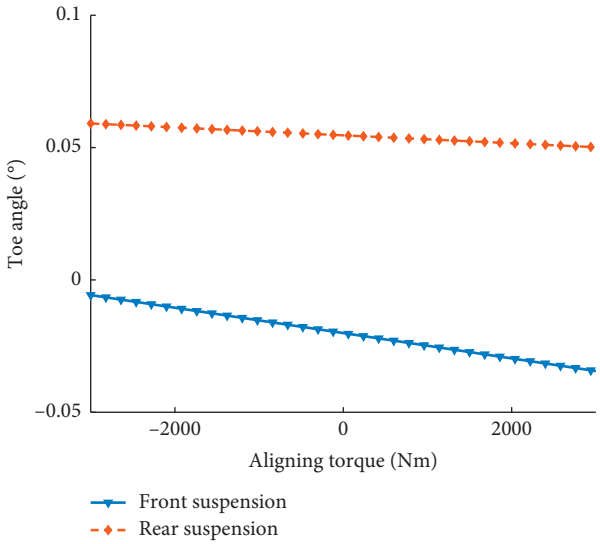

FIGURE 15: The change of the car's toe angle with the aligning force.

front and rear tires, respectively. σ_f and σ_r are the camber angles of front and rear tires.

After performing the opposite travel simulation on the vehicle's front and rear suspension's multibody dynamics models established in Figures 4 and 5, the curve of the wheel's camber angle with wheel's displacement is shown in Figure 16 is obtained [17]. In Figure 16, when the wheels bounce down, the camber angles of the front and rear suspension wheels (the inner wheel when turning) change to the positive camber direction. When the wheels jump up, the camber angles of the wheels (outer wheels when turning) of the front suspension and the rear suspension both change in the direction of negative camber. In terms of adhesion, whether it is the front suspension's or the rear suspension's outer wheel camber angle changing to the negative camber direction, the tire adhesion will be improved. From the perspective of understeer characteristics of the car, when the car is turning, the camber angle of the outer wheels of the front suspension changes to the negative camber direction, which will reduce the understeer characteristic of the car, and the camber angle of the outer wheels of the rear suspension changes to the negative camber direction, which will increase the understeer characteristics of the car.

From equations (23), (26), and (27), the front wheel's steering force caused by the change of toe angle is

$$\begin{aligned} Y_{f1} + Y_{f2} &= K_{f1}\alpha_{f1} + K_{f2}\alpha_{f2} \\ &= 2K_{f0}\left[1 - \frac{\partial K_f}{\partial W}\frac{\Delta W}{2K_{f0}} - \frac{1}{2}\left(\frac{2X_f}{\mu W_f}\right)^2\right] \\ &\quad \times \left[\frac{\partial \alpha_f}{\partial z}\frac{t_f hW}{2K_\phi}y - \frac{\partial \alpha_f}{\partial T}\left(\xi + \frac{\alpha_c W}{2K_y}x\right)\frac{bW}{l}y\right] \\ &\quad - 2K_{f0}\left(\frac{\partial \alpha_f}{\partial z}\frac{ahW}{K_\theta}x - \frac{\partial \alpha_f}{\partial X}\frac{\alpha_c W}{2}x\right)\frac{\partial K_f}{\partial W}\frac{\Delta W_f}{K_{f0}} \\ &\approx 2K_f^*\left[\frac{\partial \alpha_f}{\partial z}\right]\frac{t_f hW}{2K_\phi} - \frac{\partial \alpha_f}{\partial T}\left(\xi + \frac{\alpha_c W}{2K_y}x\right)\frac{bW}{l}y\left[-\left(\frac{\partial \alpha_f}{\partial z}\frac{l_f hW}{K_\theta}x - \frac{\partial \alpha_f}{\partial X}\frac{\alpha_c W}{2}x\right)\frac{\partial K_f}{\partial W}\frac{\Delta W_f}{K_{f0}}\right] \\ &= 2K_f^* a_f. \end{aligned} \tag{32}$$

Similarly, for the rear wheels,

$$\begin{aligned} Y_{r1} + Y_{r2} &= K_{r1}\alpha_{r1} + K_{r1}\alpha_{r2} \\ &\approx 2K_r^*\left[\frac{\partial \alpha_r}{\partial z}\frac{bhW}{K_\theta}\ddot{y} + \left(\frac{\partial \alpha_r}{\partial z}\frac{bhW}{2K_\theta}\ddot{x} + \frac{\partial \alpha_r}{\partial X}\frac{1-\alpha_c}{2}W\ddot{x}\right)\frac{\partial K_r}{\partial W}\frac{\Delta W_r}{K_{r0}}\right] \\ &= 2K_r^*\alpha_r. \end{aligned} \tag{33}$$

In the above equations, tiny quantities of order 2 and above are omitted for small longitudinal and lateral accelerations.

In the above derivation process of equations (32) and (33), the changes of toe angles $(\alpha_{f1}, \alpha_{f2})$ and deformation steering angle $(\alpha_{r1}, \alpha_{r2})$ of the front and rear wheels are

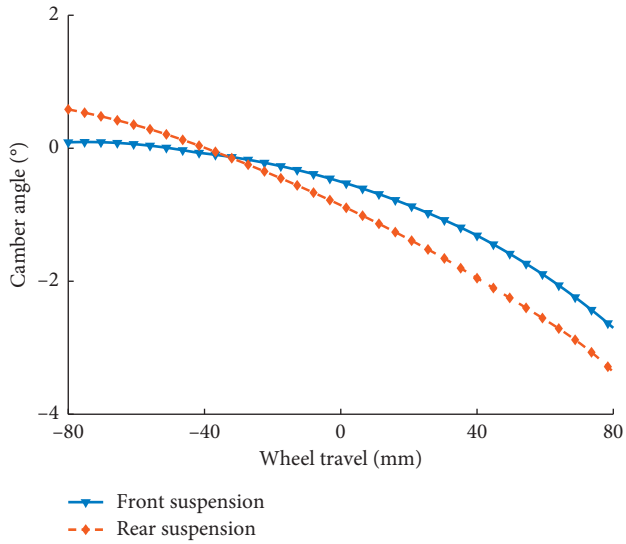

Figure 16: Curves of the suspension's camber angle with wheel's displacement.

replaced by a single equivalent angle (α_f, α_r). Sum up, the lateral force caused by suspension of vehicle is

$$F_{y1} = 2K_f^*\alpha_f + 2K_r^*\alpha_r + 2Y_{cf} + 2Y_{cr}. \quad (34)$$

8. Establishment of Simplified Car Dynamics Model

The car itself is a complex nonlinear dynamic system, it is difficult to describe it accurately with formulas. However, in order to reflect the performance of the car under some special working conditions, after omitting some minor parts of the complex automobile system, a simplified 5-DOF vehicle dynamic model is established. The model's degrees of freedom include three angular motions of the sprung mass (roll, pitch, and yaw) and two planar motions of the unsprung mass (longitudinal and lateral) [1, 18].

8.1. Kinematics Analysis of Vehicle. In the vehicle's course of motion, the lateral acceleration and longitudinal acceleration will change, and the sprung mass will move relative to unsprung mass. The sprung mass center O_s and unsprung mass center O_u of the car are shown in Figure 17.

In Figure 17, h_p is the height from pitch center O_p to the mass center of sprung mass O_s; e is the height from the unsprung's mass center to the ground; C_1 is the distance from the unsprung's mass center to the pitch center; and C_2 is the distance from the mass center of sprung to the pitch center.

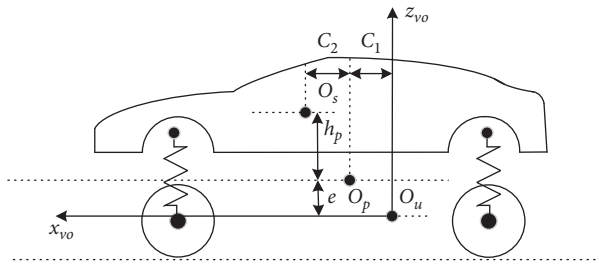

Figure 17: The center of mass of body's different parts.

As shown in Figure 18, α is side slip angle of front wheels. ψ is the yaw angle of the car's unsprung mass. δ_f is the steering angle of the car's front wheels. α_f is the side slip angle of the car's front tires. β is the side slip angle of the car's center of mass.

The longitudinal speed u and lateral speed v of the unsprung mass can be calculated by

$$\begin{cases} \dot{X} = u\cos\psi - v\sin\psi, \\ \dot{Y} = u\sin\psi + v\cos\psi. \end{cases} \quad (35)$$

The longitudinal and lateral accelerations of the unsprung mass can be calculated by

$$\begin{cases} (a_{Ou})_x = \ddot{X}\cos\psi + \ddot{Y}\sin\psi = \dot{u} - \dot{\psi}v, \\ (a_{Ou})_y = -\ddot{X}\sin\psi + \ddot{Y}\cos\psi = \dot{v} + \dot{\psi}u. \end{cases} \quad (36)$$

The acceleration vector of vehicle's sprung mass $\vec{a}_{Os}$ is obtained by summing the vector of the vehicle's unsprung mass acceleration $\vec{a}_{Ou}$, the relative acceleration $\vec{a}_{Os/Ou}$, the Coriolis acceleration $\vec{a}_C$, and the implicated acceleration $\vec{a}_{\text{Trac}}$:

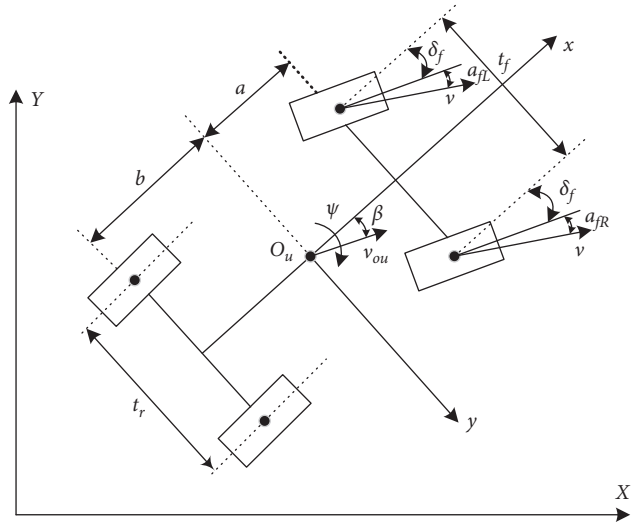

Figure 18: Side slip angle of front wheels.

$$\vec{a}_{Os} = \vec{a}_{Ou} + \vec{a}_{Os/Ou} + \vec{a}_C + \vec{a}_{\text{Trac}} = A_i\hat{i} + A_j\hat{j} + A_k\hat{k}. \tag{37}$$

Among them,

$$\begin{cases} \vec{a}_C = 2\dot{\psi}\hat{k} \times \vec{v}_{Os/Ou}; \quad \vec{a}_{Trac} = (\vec{a}_{\text{Trac}})_n + (\vec{a}_{\text{Trac}})_t, \\ (\vec{a}_{\text{Trac}})_n = \dot{\psi}\hat{k} \times \left(\dot{\psi}\hat{k}t \times n\vec{r}_{Os/Ou}\right); \quad (\vec{a}_{\text{Trac}})_t = \psi\hat{k} \times \vec{r}_{Os/Ou}, \end{cases} \tag{38}$$

$$\begin{cases} A_i = -C_2\dot{\theta}^2\cos\theta - C_2\theta\sin\theta - \dot{\psi}^2\left(C_1 + C_2\cos\theta + h_p\cos\phi sin\theta\right) + \psi h_p\sin\phi + 2\dot{\psi}h_p\dot{\phi}\cos\phi \\ - h_p\left[\left(\dot{\phi}^2\cos\phi + \phi\sin\phi\right)\sin\theta + 2\dot{\theta}\dot{\phi}\sin\phi\cos\theta\right. \\ \left. + \dot{\theta}^2\cos\phi\sin\theta - \theta\cos\theta\cos\phi\right] + \dot{u} - v\dot{\psi}, \\ A_j = h_p\left[\dot{\phi}^2\sin\phi - \phi\cos\phi + \dot{\psi}^2\sin\phi\right] \\ + \dot{\psi}\left(C_1 + C_2\cos\theta + h_p\cos\phi\sin\theta\right) \\ - 2\dot{\psi}\left(C_2\dot{\theta}\sin\theta + h_p\dot{\phi}\sin\phi\sin\theta - h_p\dot{\theta}\cos\phi\cos\theta\right) \\ + \dot{v} + u\dot{\psi}, \\ A_k = -h_p\left(\dot{\theta}^2\cos\theta\cos\phi + \theta\sin\theta\cos\phi - 2\theta\dot{\phi}\sin\theta\sin\phi + \phi\cos\theta\sin\phi\right)C_2\dot{\theta}^2\cos\theta \\ + C_2\theta\sin\theta. \end{cases} \tag{39}$$

8.2. Dynamics Analysis of Vehicle. On the basis of the lateral stiffness, lateral force, and automobile's kinematics analysis, the force of the vehicle can be obtained.

In equation (39), A_i, A_j, A_k are the accelerations of the sprung mass in the three directions x, y, z. $\vec{r}_{Os/Ou}$ is the distance between the sprung mass center and the unsprung mass center. θ is the angle of the car's sprung mass rotates relative to the unsprung mass around the x-axis, also known as the pitch angle. ϕ is the angle by which the sprung mass of the car rotates relative to the unsprung mass about the y-axis, also known as the roll angle. From these acceleration components, the inertial force of the vehicle's body and the inertial force of the unsprung mass can be expressed as

$$\begin{cases} F_s = -m_s\left(A_i i + A_j j + A_k k\right), \\ F_u = -m_u\left((\dot{u} - \dot{\psi}v)i + (\dot{v} + \dot{\psi}u)j\right), \end{cases} \tag{40}$$

where m_s is the sprung mass of the car. m_u is the unsprung mass of the car. The longitudinal force, lateral force, and inertia force of the wheel are shown in Figure 19.

In Figure 19, F_{iz} is the vertical force on the tires. F_y is the lateral force, and X_{it} is the longitudinal force on the tires, where $i = fR, fL, rR, rL$. O_p is pitch center, and O_s is the

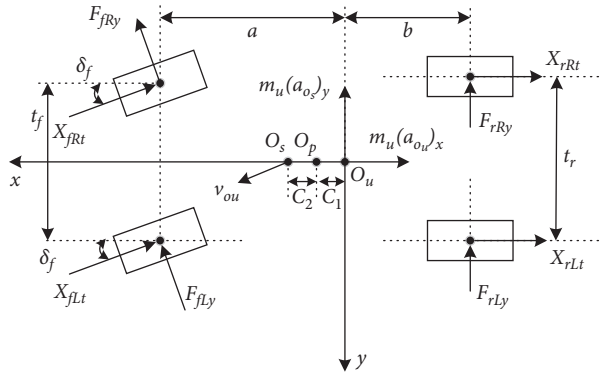

Figure 19: Model of vehicle subjected to external and inertial forces.

mass center of sprung mass. Considering the external force of the entire vehicle, the equation of motion can be summarized as [19]

$$\begin{cases} m_u v\left(\dfrac{d\beta}{dt} - \dfrac{d\psi}{dt}\right) + m_s A_i + \left(F_{fLy} + F_{fRy}\right)\sin\delta_f + X_{fLt} + X_{fRt} - X_{rLt} + X_{rRt} = 0, \\ m_u u\left(\dfrac{d\beta}{dt} + \dfrac{d\psi}{dt}\right) + m_s A_j - \left(F_{fLy} + F_{fRy}\right)cos\delta_f - F_{rLy} - F_{rRy} + \left(X_{fLt} + X_{fRt}\right)sin\delta_f = 0, \\ I_x\dfrac{d^2\phi}{dt^2} - I_{xz}\dfrac{d^2\psi}{dt^2} + m_s A_k h_p \sin\phi - m_s h_p g \sin\phi + \dfrac{1}{2}t_f\left(F_{fLz} - F_{fRz}\right) + \dfrac{1}{2}t_r\left(F_{rLz} - F_{rRz}\right) + m_s A_j\left(e - C_2\cos\theta + h\cos\theta\cos\phi\right) = 0, \\ I_y\dfrac{d^2\theta}{dt^2} + m_s A_k\left(C_1 + C_2\cos\theta + h_p\cos\phi\sin\theta\right) - m_s A_i\left(e - C_2\cos\theta + h_p\cos\theta\cos\phi\right) - m_s h_p g\sin\theta\sin\phi + a\left(F_{fLz} + F_{fRz}\right) - b\left(F_{rLz} + F_{rRz}\right) = 0, \\ I_z\dfrac{d^2\psi}{dt^2} - I_{xz}\dfrac{d^2\phi}{dt^2} = m_s A_i h_p \sin\phi + m_s A_j\left(C_1 + C_2\cos\theta + h_p\cos\phi\sin\theta\right) - \dfrac{1}{2}t_f\left(F_{fRy} - F_{fLy}\right)\sin\delta_f - b\left(F_{rRy} + F_{rLy}\right) \\ -\dfrac{1}{2}t_f\left(X_{fRt} - X_{fLt}\right)cos\delta_f - a\left(X_{fRt} + X_{fLt}\right)sin\delta_f + a\left(F_{fRy} + F_{fLy}\right)\cos\delta_f + \dfrac{1}{2}t_r\left(X_{rRt} - X_{rLt}\right). \end{cases} \tag{41}$$

8.3. Simplified Vehicle Dynamics Model. Because this paper uses the sine-swept steering input simulation, the longitudinal speed of the car remains the same in the whole process of the vehicle's movement. So vehicle's pitch degree of freedom is omitted.

If the vehicle's speed remains constant, the vehicle's longitudinal forces X_{fLt}, X_{fRt}, X_{rLt}, and X_{rRt} are ignored, and the car's roll steering and roll camber are only considered. So the longitudinal acceleration $\ddot{x}$ is zero, and then the model can be simplified into a 3-DOF vehicle dynamics

model including roll degrees of freedom, lateral degrees of freedom, and yaw degrees of freedom. Combining equations (32) and (33), the sum of the lateral force F_{y1} caused by the suspension and the lateral force F_{y2} caused by the tire is the total lateral force acting on the vehicle's tires:

$$\begin{aligned}\sum F_y &= F_{y1} + F_{y2} = 2Y_f + 2Y_r + 2Y_{cf} + 2Y_{cr} + F_{y2} \\ &= 2K_f^*\left[\frac{\partial \alpha_f}{\partial z}\frac{t_f hW}{2K_\phi} - \frac{\partial \alpha_f}{\partial T}\frac{bW}{l}\xi\ddot{y} - \frac{\partial \alpha_f}{\partial T}\frac{bW}{l}\frac{\alpha_c W}{2K_y}\ddot{y}\ddot{x} - \left(\frac{\partial \alpha_f}{\partial z}\frac{l_f hW}{K_\theta}\ddot{x} - \frac{\partial \alpha_f}{\partial X}\frac{\alpha_c W}{2}\ddot{x}\right)\frac{\partial K_f}{\partial W}\frac{\Delta W_f}{K_{f0}}\right] \\ &\quad + 2K_r^*\left[\frac{\partial \alpha_r}{\partial z}\frac{bhW}{K_\theta}\ddot{y} + \left(\frac{\partial \alpha_r}{\partial z}\frac{bhW}{2K_\theta}\ddot{x} + \frac{\partial \alpha_r}{\partial X}\frac{1-\alpha_c}{2}W\ddot{x}\right)\frac{\partial K_r}{\partial W}\frac{\Delta W_r}{K_{r0}}\right] - 2K_{cf}\frac{\partial \sigma_f}{\partial \phi}\phi - 2K_{cr}\frac{\partial \sigma_r}{\partial \phi}\phi \\ &\quad + \left\{2K_f^*\left(\delta - \beta - \frac{a}{u}\dot{\psi}\right) + 2K_r^*\left(\beta + \frac{b}{u}\dot{\psi}\right)\right\}.\end{aligned} \tag{42}$$

Due to only the car's roll steering and roll camber are considered, the car's aligning torque is ignored, combining to equation (24), and then equation (42) becomes:

$$\begin{aligned}\sum F_y &= F_{y1} + F_{y2} = 2Y_f + 2Y_r + 2Y_{cf} + 2Y_{cr} + F_{y2} \\ &= \left\{2K_{f0}\frac{\partial \alpha_f}{\partial \phi}\phi_s + 2K_{r0}\frac{\partial \alpha_r}{\partial \phi}\phi - 2K_{cf}\frac{\partial \sigma_f}{\partial \phi}\phi - 2K_{cr}\frac{\partial \sigma_r}{\partial \phi}\phi\right\} + \left\{2K_{f0}\left(\delta - \beta - \frac{a}{u}\dot{\psi}\right) + 2K_{r0}\left(\beta + \frac{b}{u}\dot{\psi}\right)\right\}.\end{aligned} \tag{43}$$

Combining equations (24) and (43), the dynamic equation of the model is as follows:

$$\begin{cases}(m_s + m_u)u\dfrac{d\beta}{dt} + 2\left(K_{f0} + K_{r0}\right)\beta + \left[(m_s + m_u)u + \dfrac{2\left(aK_{f0} - bK_{r0}\right)}{u}\right]\dot{\psi} - m_s h_s\dfrac{d^2\phi}{dt^2} - 2Y_\phi\phi = 2K_f\delta, \\ 2\left(aK_{f0} - bK_{r0}\right)\beta + I_z\dfrac{d\dot{\psi}}{dt} + \dfrac{2\left(a^2K_{f0} - b^2K_{r0}\right)}{v}\dot{\psi} - I_{xz}\dfrac{d^2\phi}{dt^2} - 2N_\phi\phi = 2aK_{f0}\delta, \\ -m_s h_s u\dfrac{d\beta}{dt} - I_{xz}\dfrac{d\dot{\psi}}{dt} - m_s h_s u\dot{\psi} + I_x\dfrac{d^2\phi}{dt^2} + C_\phi\dfrac{d\phi}{dt} + \left(K_\phi - m_s g h_s\right)\phi = 0.\end{cases} \tag{44}$$

Among them,

$$\begin{cases} Y_\phi = \left(\dfrac{\partial \alpha_f}{\partial \phi}K_f + \dfrac{\partial \alpha_r}{\partial \phi}K_r\right) - \left(\dfrac{\partial \sigma_f}{\partial \phi}K_{cf} + \dfrac{\partial \sigma_r}{\partial \phi}K_{cr}\right), \\ N_\phi = \left(\dfrac{\partial \alpha_f}{\partial \phi}aK_f - \dfrac{\partial \alpha_r}{\partial \phi}bK_r\right) - \left(\dfrac{\partial \sigma_f}{\partial \phi}aK_{cf} - \dfrac{\partial \sigma_r}{\partial \phi}bK_{cr}\right). \end{cases} \tag{45}$$

Performing Laplace transformation on equations (44), the following equations represented by a matrix are obtained:

$$\begin{bmatrix} (m_s+m_u)us + 2\left(K_{f0}+K_{r0}\right) & (m_s+m_u)u + \dfrac{2\left(aK_{f0}-bK_{r0}\right)}{u} & -m_s h_s s^2 - 2Y_\phi \\ 2\left(aK_{f0}-bK_{r0}\right) & I_z s + \dfrac{2a^2K_{f0}+b^2K_{r0}}{u} & -I_{xz}s^2 - 2N_\phi \\ -m_s h_s us & -I_{xz}s - m_s h_s u & I_x s^2 + C_\phi s + \left(K_\phi - m_s g h_s\right) \end{bmatrix} \begin{bmatrix} \beta \\ \dot{\psi} \\ \phi \end{bmatrix} = \begin{bmatrix} 2K_{f0}\delta(s) \\ 2aK_{f0}\delta(s) \\ 0 \end{bmatrix}. \tag{46}$$

The transfer function can be obtained from equation (46):

$$\frac{\beta(s)}{\delta(s)} = \frac{\begin{vmatrix} 2K_{f0} & (m_s+m_u)u + \left(\left(2\left(aK_{f0}-bK_{r0}\right)\right)/u\right) & -m_s h_s s^2 - 2Y_\phi \\ 2aK_{f0} & I_z s + \left(\left(2a^2K_{f0}+b^2K_{r0}\right)/u\right) & -I_{xz}s^2 - 2N_\phi \\ 0 & -I_{xz}s - m_s h_s v & I_x s^2 + C_\phi s + \left(K_\phi - m_s g h_s\right) \end{vmatrix}}{\begin{vmatrix} (m_s+m_u)us + 2\left(K_{f0}+K_{r0}\right) & (m_s+m_u)u + \left(\left(2\left(aK_{f0}-bK_{r0}\right)\right)/u\right) & -m_s h_s s^2 - 2Y_\phi \\ 2\left(aK_{f0}-bK_{r0}\right) & I_z s + \left(\left(2a^2K_{f0}+b^2K_{r0}\right)/u\right) & -I_{xz}s^2 - 2N_\phi \\ -m_s h_s us & -I_{xz}s - m_s h_s u & I_x s^2 + C_\phi s + \left(K_\phi - m_s g h_s\right) \end{vmatrix}}, \tag{47}$$

$$\frac{\dot{\psi}(s)}{\delta(s)} = \frac{\begin{vmatrix} (m_s+m_u)us + 2\left(K_{f0}+K_{r0}\right) & 2K_{f0} & -m_s h_s s^2 - 2Y_\phi \\ 2\left(aK_{f0}-bK_{r0}\right) & 2aK_{f0} & -I_{xz}s^2 - 2N_\phi \\ -m_s h_s us & 0 & I_x s^2 + C_\phi s + \left(K_\phi - m_s g h_s\right) \end{vmatrix}}{\begin{vmatrix} (m_s+m_u)us + 2\left(K_{f0}+K_{r0}\right) & (m_s+m_u)u + \left(\left(2\left(aK_{f0}-bK_{r0}\right)\right)/u\right) & -m_s h_s s^2 - 2Y_\phi \\ 2\left(aK_{f0}-bK_{r0}\right) & I_z s + \left(\left(2a^2K_{f0}+b^2K_{r0}\right)/u\right) & -I_{xz}s^2 - 2N_\phi \\ -m_s h_s us & -I_{xz}s - m_s h_s u & I_x s^2 + C_\phi s + \left(K_\phi - m_s g h_s\right) \end{vmatrix}}, \tag{48}$$

$$\frac{\phi(s)}{\delta(s)} = \frac{\begin{vmatrix} (m_s+m_u)us + 2\left(K_{f0}+K_{r0}\right) & (m_s+m_u)u + \left(\left(2\left(aK_{f0}-bK_{r0}\right)\right)/u\right) & 2K_{f0} \\ 2\left(aK_{f0}-bK_{r0}\right) & I_z s + \left(\left(2a^2K_{f0}+b^2K_r\right)/u\right) & 2aK_{f0} \\ -m_s h_s us & -I_{xz}s - m_s h_s u & 0 \end{vmatrix}}{\begin{vmatrix} (m_s+m_u)us + 2\left(K_{f0}+K_{r0}\right) & (m_s+m_u)u + \left(\left(2\left(aK_{f0}-bK_{r0}\right)\right)/u\right) & -m_s h_s s^2 - 2Y_\phi \\ 2\left(aK_{f0}-bK_{r0}\right) & I_z s + \left(\left(2a^2K_{f0}+b^2K_{r0}\right)/u\right) & -I_{xz}s^2 - 2N_\phi \\ -m_s h_s us & -I_{xz}s - m_s h_s u & I_x s^2 + C_\phi s + \left(K_\phi - m_s g h_s\right) \end{vmatrix}}, \tag{49}$$

where $K_{\phi f}$ is the roll stiffness of the front suspension and $K_{\phi r}$ is the roll stiffness of the rear suspension. $K_{\phi f}$ includes the front suspension's spring stiffness $K_{\phi fs}$ and the antiroll bar's stiffness $K_{\phi fw}$. The stiffness $K_{\phi r}$ includes the rear suspension's spring stiffness $K_{\phi rs}$ and the stiffness $K_{\phi rw}$ of the rear antiroll bar. Substitute equations (3) and (4) into equations (47)–(49), the transfer function of response indicators that couple stiffness of the spring and the antiroll bar relative to the steering wheel angle is obtained.

9. Build the Vehicle's Dynamics Model and Multitarget Optimization

The impact of the suspension on the tire's force can be known from the previous analysis. The load transfer will cause the tire's side slip stiffness to change, and the longitudinal force and lateral force will cause the toe angle change and deformation steering of the tire. The influence of suspension on the side slip stiffness and the tire's steering angle can be equivalent to the lateral force generated by the deformation of the automobile's tire.

9.1. Build the Car's Dynamics Model. In order to analyze and simulate the vehicle's handling stability, based on the above analysis of vehicle's dynamics, a vehicle's dynamic model was established in ADAMS/CAR software. The established vehicle's dynamic model includes a front suspension system, a rear suspension system, a steering system, and a braking system.

The tire's Magic formula was used in building the tire's dynamics model. The lateral force of a car's tire can be obtained by the Magic formula:

$$F_{ijy} = F_{ijz} \sin\left\{D_t \tan^{-1}\left[B_{it}\alpha_{ij} - E_t\left(B_{it}\alpha_{ij} - \tan^{-1}\left(B_{it}\alpha_{ij}\right)\right)\right]\right\} + \gamma_{ij}\left(\varepsilon_1 F_{ijz} + \varepsilon_2\right), \tag{50}$$

where i and j are the labels for the wheels, $i = f, r$, $j = R, L$. The coefficients D_t, B_{it}, and E_t need to be measured through actual experiment and have no practical physical significance. The side slip angle α_{fj} of the front wheels and the side slip angle α_{rj} of the rear wheels can be calculated by the following formulas:

$$\begin{cases} \alpha_{fj} = \tan^{-1}\left[\dfrac{2v + 2a\dot{\psi}}{2u + \beta_1 t_f \dot{\psi}}\right] - \delta_f, \\ \alpha_{rj} = \tan^{-1}\left[\dfrac{2v - 2b\dot{\psi}}{2u + \beta_1 t_r \dot{\psi}}\right], \end{cases} \quad (j = R, L), \tag{51}$$

$$\beta_1 = \begin{cases} +1, & j = L, \\ -1, & j = R. \end{cases}$$

The longitudinal force of a car's tires depends on the vehicle's forward acceleration and whether the tire is a driving wheel. Considering the longitudinal force of the car and the force of the tire, the equation of motion of the car's tire can be obtained.

The motion equation of the driving wheel is

$$I_r \dot{\tau}_{rj} = T_d - rX_{rjt} - \varepsilon F_{rjz}, \quad j = R, L. \tag{52}$$

The motion equation of the slave wheel is

$$I_f \dot{\tau}_{fj} = rX_{rjt} - \varepsilon F_{fjz}, \quad j = R, L. \tag{53}$$

In equations (52) and (53), F_{iz} is the vertical force on the wheels, and X_{it} is the longitudinal force on the wheels, $i = fR, fL, rR, rL$. I_f and I_r are the moment inertia of front and rear wheels. τ is the angular velocity of wheels. r is wheels' radius. T_d is the driving torque. ε is rolling resistance of wheels. The vertical displacement d_{it} between the connection point of the spring and the damper caused by the roll and pitch movement of the car and the vertical speed v_{ij} of the sprung mass can be calculated by the following formulas:

$$\begin{aligned} d_{ij} &= -p_1 \sin\theta + \frac{1}{2} t_i p_2 \sin\phi\cos\theta + h_z(\cos\theta\cos\phi - 1), \\ v_{ij} &= \frac{1}{2} t_i p_2 \dot{\phi}\cos\theta - p_2 p_1 \dot{\theta}, \end{aligned} \tag{54}$$

where

$$\begin{aligned} p_1 &= \begin{cases} a, & i = f, \\ b, & i = r, \end{cases} \\ p_2 &= \begin{cases} -1, & j = R, \\ 1, & j = L, \end{cases} \end{aligned} \tag{55}$$

The vertical load on each wheel is

$$F_{ijz} = (m_s + m_u) g \frac{\xi_1 a + \xi_2 b}{a + b} + d_{ij} k_i + v_{ij} c_i, \tag{56}$$

where

$$\begin{aligned} \xi_1 &= \begin{cases} 0, & i = f, \\ 1, & i = r, \end{cases} \\ \xi_2 &= \begin{cases} 1, & j = R, \\ 0, & i = r. \end{cases} \end{aligned} \tag{57}$$

For pure rotation of each wheel, its angular velocity can be expressed as

$$\tau_{ij} = \frac{1}{R}\sqrt{\left(\frac{u + \beta_2 \dot{\psi} t_i}{2}\right)^2 + \left(v + \beta_1 a \dot{\psi}\right)^2}, \tag{58}$$

where

$$\beta_1 = \begin{cases} 1, & i = f, \\ -1, & i = r, \end{cases} \qquad \beta_2 = \begin{cases} 1, & j = L, \\ -1, & j = R. \end{cases} \tag{59}$$

The parameters of the vehicle's dynamics model finally established are shown in Table 1.

This article uses the sine-swept steering input simulation method to evaluate the handling stability of the car; that is, the steering wheel angle's input waveform is changed to a sine wave. Using sine wave input with different frequencies, the amplitude ratio of the output to the input at different frequencies can be obtained, that is, the amplitude-frequency characteristics of the car. At the same time, the phase difference between the output and the input at different frequencies can be obtained, that is, the phase frequency characteristics of the car. The simulation data of the sine-swept steering input simulation in this paper are shown in Table 2.

Table 1: Vehicle's parameters.

Parameter	Value
m_s (kg)	1067
m_u (kg)	595
A (mm)	1452.6
B (mm)	1249.5
t_f (mm)	1508.3
t_r (mm)	1487.8
m_f (kg)	891.89
k_{tf} (N/mm)	210
$k_{\phi fs}$ (N/mm)	43
$k_{\phi rs}$ (N/mm	32
$k_{\phi wf}$ (N/mm)	29400
$k_{\phi wr}$ (N/mm)	12800
h_s (mm)	330
l (mm)	2702.1
m_r (kg)	770.11
k_{tr} (N/mm)	240

Table 2: The simulation parameters.

Parameter	Value
Time (s)	20
Steps	2048
Velocity (km/h)	100
Max steer wheel angle (°)	24.5
Initial frequency (Hz)	0.2
Max frequency (Hz)	3.8
Frequency rate (Hz/s)	0.2
Start time (s)	2

9.2. Set Up Multiple Target Optimization Functions. In equations (48)–(50), make $s = j\omega$ and $j = \sqrt{-1}$, the frequency response characteristic function of the car can be obtained, including amplitude-frequency characteristics and phase frequency characteristics. $|\dot{\psi}/\delta(\omega)|$, $|\phi/\delta(\omega)|$, and $|\beta/\delta(\omega)|$ are the gain of yaw rate, roll angle, and side slip angle relative to the steering wheel angle in the amplitude-frequency characteristic function. $\rho_\psi(\omega)$, $\rho_\phi(\omega)$, and $\rho_\beta(\omega)$ are the corresponding phase lag angles. The frequency corresponding to the maximum gain of the yaw rate relative to the steering wheel angle is the resonance frequency of the car. The phase lag angle can be converted into the delay time by the following formula:

$$t = \frac{\rho + 180}{360 \cdot \omega} \quad \text{or} \quad \frac{\rho - 180}{360 \cdot \omega}. \tag{60}$$

Because the frequency of driver rotates the steering wheel is about 0.5 Hz. Based on the theoretical analysis of the above part, in the sine-swept steering input simulation, the yaw rate gain relative to the steering wheel angle at 0.5 Hz, the resonance frequency f_ψ, roll angle gain relative to the steering wheel angle, the delay time t_1 of lateral acceleration relative to the steering wheel angle, and the delay time t_2 of yaw rate relative to lateral acceleration are used as optimized target. The stiffness of suspension's spring and the antiroll bar are used as the optimized variables to do multiobjective optimization [20, 21].

In order to achieve a better handling stability of the car, the yaw rate gain relative to the steering wheel angle, the roll angle gain relative to the steering wheel angle, the side slip angle gain relative to the steering wheel angle, the delay time of roll angle relative to the steering wheel angle, and the delay time of yaw rate relative to the lateral acceleration should be minimum, and at the same time, it is hoped that the resonance frequency of the yaw rate relative to the steering wheel angle is the maximum; that is, the objective function can be expressed as

$$\begin{cases} f_1 = \min\left(\left|\dfrac{\dot{\psi}}{\delta}(\omega)\right|_{\omega=0.5}\right), \\ f_2 = \min\left(\left|\dfrac{\phi}{\delta}(\omega)\right|_{\omega=0.5}\right), \\ f_3 = \min\left(\left|\dfrac{\beta}{\delta}(\omega)\right|_{\omega=0.5}\right), \\ f_4 = \max\left(f_\psi\right), \\ f_5 = \min\left(t_1\right), \\ f_6 = \min\left(t_2\right). \end{cases} \tag{61}$$

9.3. Multiobjective Optimization and Optimization Results. The Pareto solution is also called nondominated solution. When there are multiple goals, due to conflicts between goals, one solution is the best on a goal and maybe the worst on the other. While improving any objective function, these solutions will necessarily weaken at least one other objective

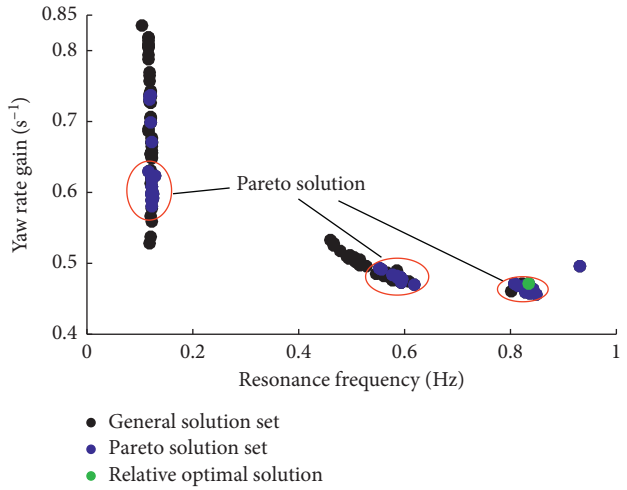

Figure 20: Pareto solution set of resonance frequency and yaw rate gain at 0.5 Hz.

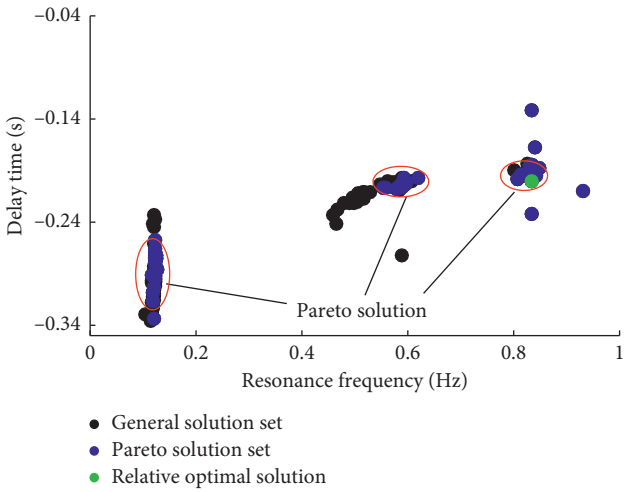

Figure 21: Pareto solution set of the delay time of lateral acceleration relative to the steering wheel angle and resonance frequency.

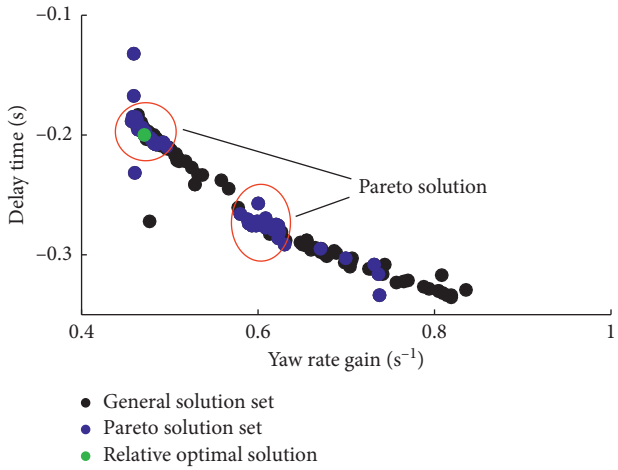

Figure 22: Pareto solution set of the delay time of yaw rate relative to lateral acceleration and resonance frequency.

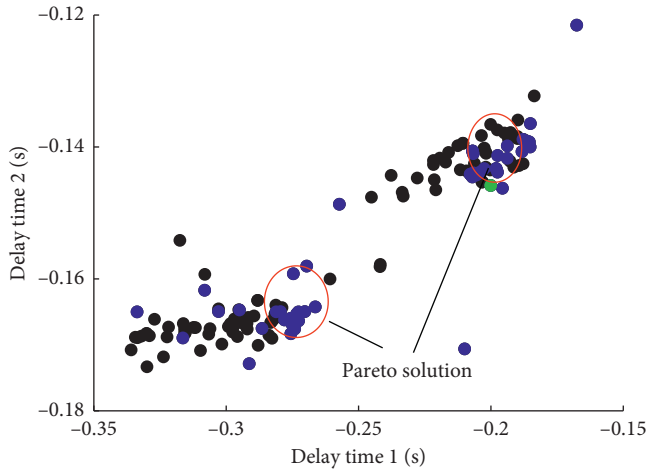

Figure 23: Pareto solution set of side slip angle gain relative to the yaw rate gain.

function, which is called a nondominated solution or a Pareto solution. The set of optimal solutions of a set of objective functions is called the Pareto solution set. In 1986, Pareto introduced the concept of a multiobjective solution, which is defined as follows: Assume that any two solutions S1 and S2 for all targets, if S1 is better than S2, then we call S1 dominate S2; if S1 is not dominated by other solutions, S1 is called a nondominated solution, also called the Pareto solution. This paper adopts multiobjective genetic algorithm to optimize the handling stability of the car.

After optimization calculation, the Pareto solution set of the vehicle's resonance frequency and yaw rate gain value at 0.5 Hz is obtained as shown in Figure 20. Figure 21 shows the Pareto solution set of resonance frequency and the delay time of lateral acceleration relative to the steering wheel angle [22].

Figure 22 is a Pareto solution set of the delay time of yaw rate relative to the lateral acceleration and the resonance frequency. Figure 23 shows the Pareto solution set of the delay time of yaw rate relative to lateral acceleration (delay time 1) and the delay time of lateral acceleration relative to steering wheel angle (delay time 2).

Figure 24 shows the Pareto solution set of the delay time of the lateral acceleration relative to the steering wheel angle and the yaw rate gain value. Figure 25 shows the Pareto solution set of side slip angle gain relative to the yaw rate gain.

As shown in Figure 26, the blue dots are the Pareto solution set of the side slip angle gain relative to the delay time of yaw rate relative to the lateral acceleration.

In the Pareto solution set of Figures 20–26, a relatively optimal solution is obtained after the optimization operation. The relatively optimal solution and two sets of solutions selected from the Pareto solution set are, respectively, brought into the vehicle model for sine-swept steering input

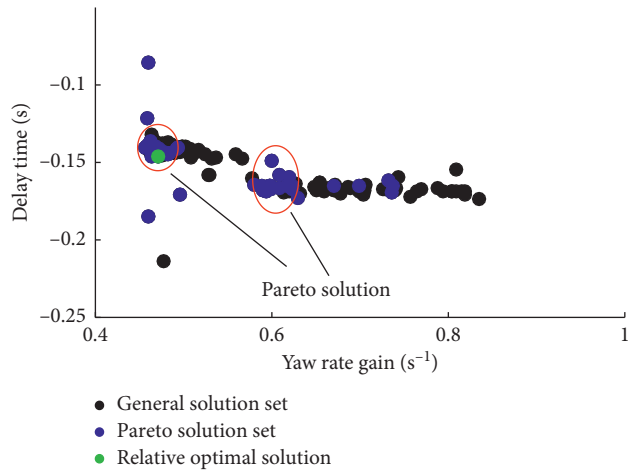

Figure 24: Pareto solution set of delay time of the lateral acceleration relative to the steering wheel angle and the yaw rate gain.

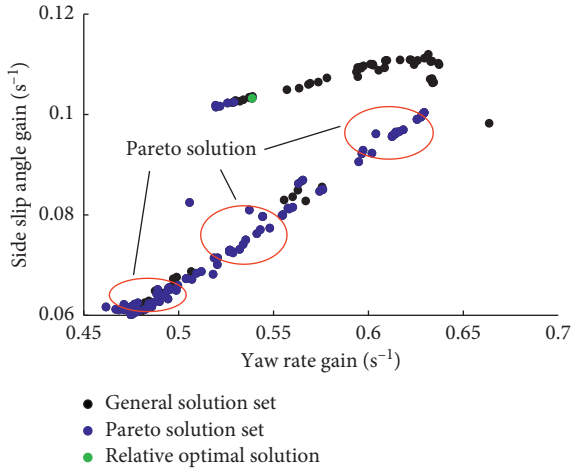

Figure 25: Pareto solution set of side slip angle gain relative to the yaw rate gain.

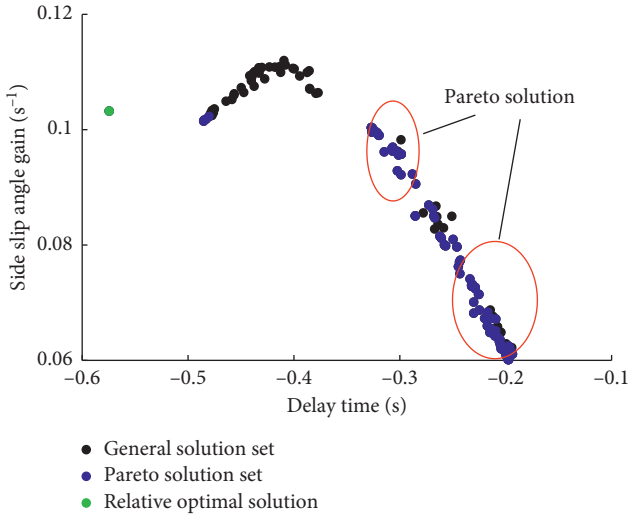

Figure 26: Pareto solution set of the side slip angle gain relative to the delay time.

simulation and then compared with the original vehicle's simulation data.

The simulation results obtained is shown in Table 3. Compared with the original car, the increase or decrease percentages of spring stiffness, antiroll bar stiffness, and optimization targets at 0.5 Hz are shown in Table 4. In Table 3, solution 1 is a relatively optimal solution, and solution 2 and solution 3 are two sets of solutions selected from the Pareto solution set.

As shown in Table 4, compared with the original car, the optimized car's front suspension spring stiffness and rear suspension spring stiffness increased by 50% and 37.5%, respectively. And the front suspension antiroll bar stiffness and rear suspension antiroll bar stiffness decreased by 10% and 28%, respectively. The yaw rate gain is reduced by 10.4%, the roll angle gain is reduced by 25%, the side slip angle gain is reduced by 17%, the resonance frequency is reduced by 3.3%, the delay time of lateral acceleration is reduced by 10%, and the delay time of yaw is reduced by 21.4%.

Table 3: The results before and after optimization.

	$k_{\phi fs}$ (N/mm)	$k_{\phi rs}$ (N/mm)	$k_{\phi fw}$ (N/mm)	$k_{\phi rw}$ (N/mm)	$f_1(s^{-1})$	$f_2(s^{-1})$	$f_3(s^{-1})$	f_4(Hz)	f_5(s)	f_6(s)
Original car	43	20	29400	12800	0.48	0.09	0.06	0.61	0.20	0.14
Solution 1	86	32	26487	9195	0.43	0.12	0.05	0.59	0.18	0.11
Solution 2	51.6	38.4	35280	15360	0.45	0.08	0.08	0.64	0.22	0.16
Solution 3	34.4	25.6	23520	10240	0.49	0.10	0.09	0.69	0.21	0.13

Table 4: The increase or decrease percentage of the optimized parameters compared with the original car.

	$k_{\phi fs}$ (N/mm)	$k_{\phi rs}$ (N/mm)	$k_{\phi fw}$ (N/mm)	$k_{\phi rw}$ (N/mm)	$f_1(s^{-1})$	$f_2(s^{-1})$	$f_3(s^{-1})$	f_4(Hz)	f_5(s)	f_6(s)
Percentage	50%	37.5%	−10%	−28%	−10.4%	−25%	−17%	−3.3%	−10%	−21.4%

After simulating the 4 sets of data in Table 3 with sine-swept steering input simulation, the comparison figures shown in Figures 27–33 were obtained. In Figures 27–33, Solution 1 is the relatively optimal solution, and Solution 2 and Solution 3 are the two sets of solutions selected from the Pareto solution set.

Figure 27 shows the curve of yaw rate gain relative to the steering wheel angle obtained after the four sets of data are brought into the model for simulation. In Figure 27, within 1 Hz, the difference between the curves is obvious. After optimization, the gain of yaw rate relative to the steering wheel at 0.5 Hz is smaller than the other three solutions, which meets the requirements of the optimization goal. Between 0 and 1 Hz, the gain value of the yaw rate relative to the steering wheel angle corresponding to the optimized scheme is smaller than the other three groups of schemes. The curve in Figure 27 has a small difference between 1 Hz and 4 Hz. Because the driver rarely exceeds the range of 1 Hz during the handling of the car, the change of the yaw rate gain value at high frequency is not important to be considered.

Figure 28 shows the phase lag of yaw rate relative to the lateral acceleration. Convert the phase lag in Figure 28 to the delay time of yaw rate relative to the lateral acceleration according to equation (60), and the delay time shown in Figure 29 can be obtained.

Figure 29 shows the delay time of the yaw rate relative to the lateral acceleration. In Figure 29, because it is a multiobjective optimization, it is difficult to make all optimization objectives reach the most ideal state. The delay time of yaw rate relative to the lateral acceleration at 0.5 Hz obtained after optimization is not much different from the other two sets of solutions. But its value is within the acceptable range. Between 0 and 1 Hz, the delay time of the yaw rate relative to the lateral acceleration corresponding to the optimized scheme was compared with the other three groups of schemes, and the result was the same as that at 0.5 Hz.

Figure 30 shows the roll angle gain relative to the lateral acceleration. In Figure 30, as the frequency increases, the curve of the roll angle gain relative to the lateral acceleration corresponding to the relatively optimal solution is smaller than the curve corresponding to the other three solutions. It shows that the obtained relatively optimal solution is beneficial to improve the handling stability of the car.

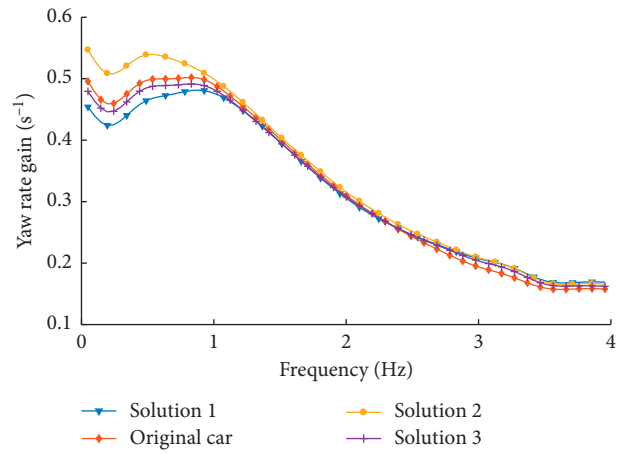

Figure 27: Yaw rate gain relative to the steering wheel angle.

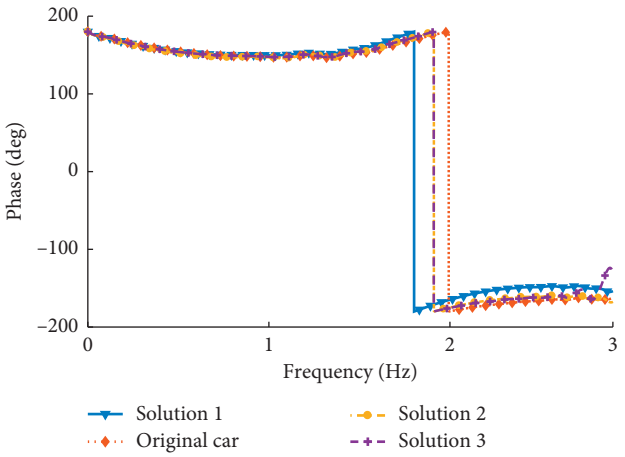

Figure 28: Phase lag of yaw rate relative to the lateral acceleration.

Figure 31 shows the delay time of lateral acceleration relative to steering wheel angle. In Figure 31, for the optimized curve, the delay time of lateral acceleration relative to the steering wheel angle at 0.5 Hz is slightly different from the curves of the other two sets of solutions, but its value is not the worst among the four sets of curves and within the acceptable range. Between 0 and 1 Hz, the delay time of the

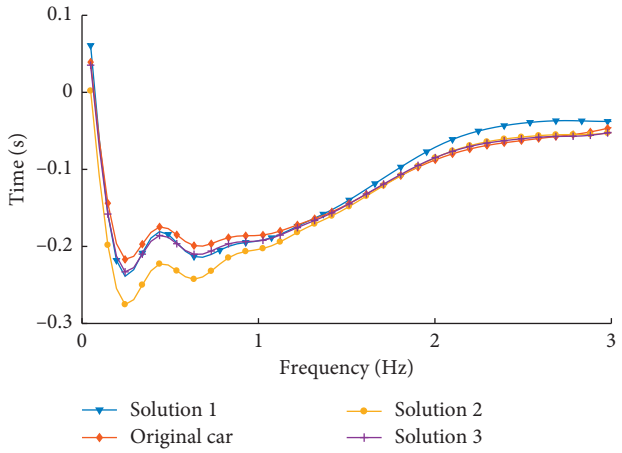

Figure 29: The delay time of yaw rate relative to lateral acceleration.

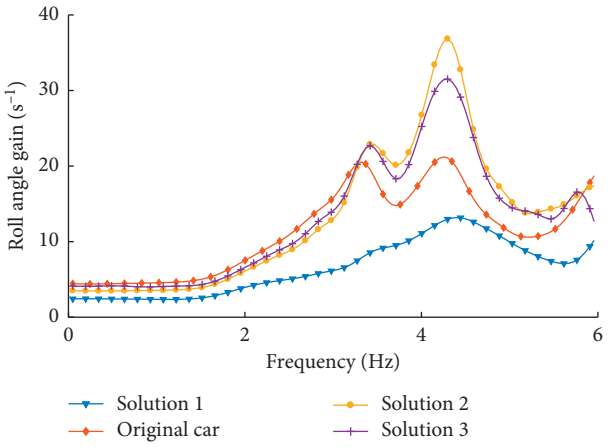

Figure 30: Roll angle gain relative to the lateral acceleration.

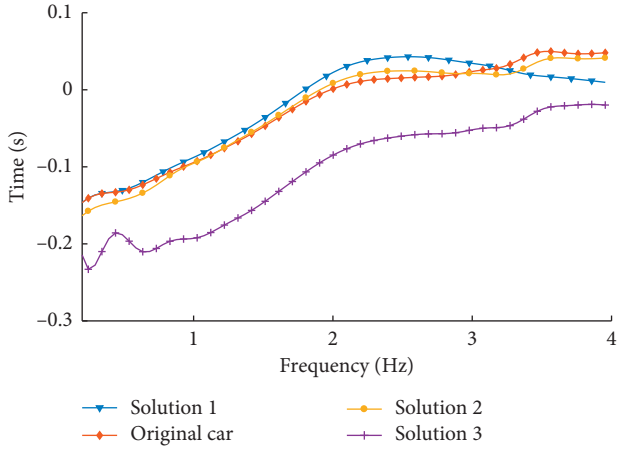

Figure 31: Delay time of lateral acceleration relative to steering wheel angle.

lateral acceleration relative to the steering wheel angle corresponding to the optimized scheme is compared with the other three schemes, and the result is the same as that at

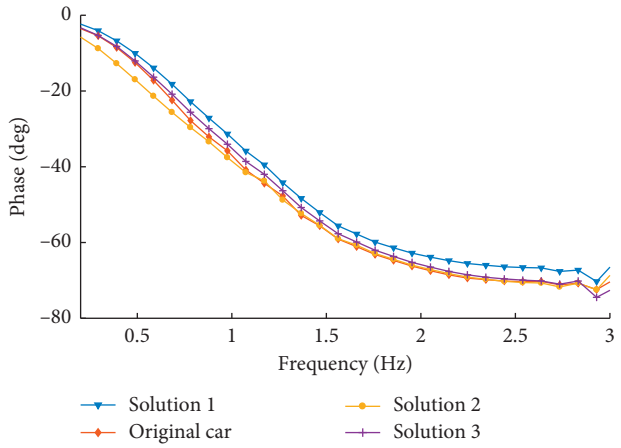

Figure 32: Phase lag of yaw rate relative to the steering angle.

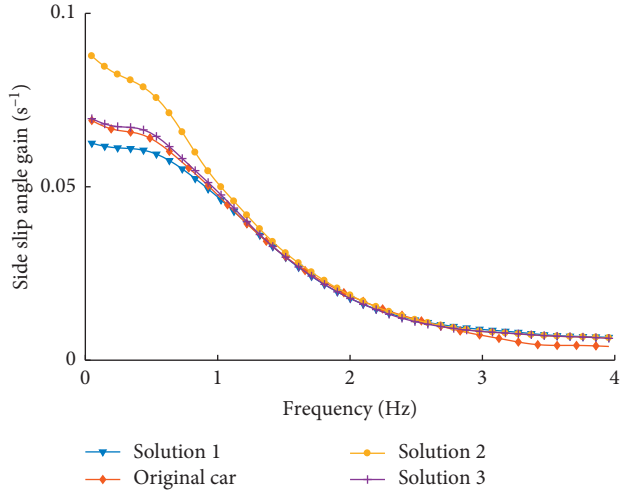

Figure 33: Side slip angle gain relative to the steering wheel angle.

0.5 Hz. As the frequency increases, the absolute value of the delay time gradually decreases. Since the driver's manipulation of the car rarely reaches more than 1 Hz, the vehicle's frequency characteristics at high frequencies are not considered.

Figure 32 shows the phase lag of yaw rate relative to the steering wheel angle. Obviously, the absolute value of the phase lag of the yaw rate relative to the steering wheel angle after the optimization is significantly reduced. This shows that the relative optimal solution of the car will make the car respond faster. This has an advantageous effect on the handling stability of the vehicle.

In Figure 33, within 1 Hz, the difference between the curves of the side slip angle gain relative to the steering wheel angle is relatively obvious, but as the frequency increases, the difference between the curves becomes smaller and smaller. The driving frequency of the general driver is generally maintained in the low frequency range, that is, within 1 Hz, so generally the car's high frequency range is not considered. Moreover, the optimized vehicle's side slip angle gain relative to the steering wheel angle at 0.5 Hz is smaller than that

of the other three solutions, which is beneficial to improve the handling stability of the vehicle and meets the requirements of the optimization goal.

10. Conclusions

In this paper, the influence mechanism of spring stiffness and antiroll bar stiffness on suspension and vehicle performance is analyzed, the simplified vehicle dynamics model is established, and the transfer function coupling spring and antiroll bar is obtained. Finally, a multibody dynamics model considering the suspension is established, and a relative optimal matching method of spring stiffness and antiroll bar stiffness is obtained through NSGA-II optimization algorithm. The specific conclusions are as follows:

(1) Suspension roll stiffness and roll center will affect the load transfer, thus changing the tire's side slip stiffness.

According to a real vehicle object studied in this paper, the law of the roll stiffness of the front and rear suspension with the spring stiffness and the stiffness of the antiroll bar is obtained. For the rear multilink suspension of the car, the instantaneous axis of motion and roll center were found through complex geometric analysis, and the law of the front and rear suspension roll center changing with wheel jump was obtained.

(2) The change of tire side slip stiffness, tire rotation angle, and camber angle caused by suspension will lead to the change of tire force.

Consider the two factors of the suspension causing the change of the tire rotation angle. One is the change of the suspension stroke caused by the vehicle's roll and pitch movement, which leads to the change of the toe angle, and this is related to the suspension's roll stiffness and pitch stiffness. On the contrary, the force received by the tire will cause a change in the rotation angle of the tire, that is deformation steering.

The influence of the suspension on the side slip stiffness and tire's rotation angle is equivalent to the lateral force generated by tire deformation plus the camber thrust generated by the camber angle to obtain the total lateral force experienced by the tire.

(3) The corresponding Pareto solution set and the relative optimal solution are obtained by using the NSGA-II algorithm to optimize. By comparison, the dynamic performance of the car is improved.

When the spring stiffness of the front suspension is increased by 50%, the stiffness of the rear suspension antiroll bar is increased by 37.5%, the stiffness of the front antiroll bar is decreased by 10%, and the spring stiffness of the rear suspension is decreased by 28%, the car's corresponding yaw rate gain, the roll angle gain and the side slip angle gain at 0.5 Hz are reduced, and the delay time of lateral acceleration and yaw rate at 0.5 Hz are within a reasonable and acceptable range. At other frequency points between 0 and 1 Hz, the results of the optimized scheme compared with the other three groups of schemes were the same as those at 0.5 Hz.

(4) The changing law of the response index under sine-swept input at low frequency and high frequency is as follows:

When the frequency is below 1 Hz, the gain and delay time do not change according to a certain law with the increase of frequency. Between 1 Hz and 3 Hz, the yaw rate gain, side slip angle gain, delay time of yaw rate, and lateral acceleration decrease as the frequency increases, and the roll angle gain increases as the frequency increases.

(5) In this paper, the optimization is carried out for the frequency point of 0.5 Hz. Next, the optimization target will be increased to a frequency range, so as to make the optimization more comprehensive and broader and improve the optimization effect.

Notation

F: Force, N
l: Wheelbase, m
r: Radius of tires, m
K: Stiffness, N · m/°
T: Torque, N · m
E: Intersection point
c: Lever's length, m
n: Lever's length, m
p: Lever's length, m
V: Velocity, m/s
m: Sprung mass, kg
h: Height, m
M: Moment, N · m
W: Vehicle's mass, kg
t: Wheel center distance, m
g: Gravitational acceleration, m/s^2
x: Longitudinal displacement, m
y: Lateral displacement, m
a: The distance between the front axle and the vehicle's center of mass, m
b: The distance between the rear axle and the vehicle's center of mass, m
X: Longitudinal force, N
z: Vertical displacement, m
Y: Lateral force, N
O: Roll center
C: Distance, m
v: Velocity, m/s
e: Distance, m
B: Coefficient of magic formula in lateral tire force
D: Coefficient of magic formula in lateral tire force
k: Stiffness, N · m/°
c: The distance between the rear axle and the vehicle's center of mass, m
A: Acceleration, m/s^2
I: Moment of inertia, m^4

f: Objective function
s: Laplace operator.
Geek symbols
η: Intersection angle, degree
ϕ: Roll angle of sprung mass, degree
Φ: Angle, degree
γ: Intersection angle, degree
β: Side slip angle of center of mass, degree
μ: Coefficient of friction between tire and ground
α: Tire's side slip angle, degree
θ: Pitch angle, degree
ξ: Tire's drag, m
δ: Front wheel steer angle, degree
ε: Rolling resistance of wheel
ψ: Yaw rate angle, degree
ω: Frequency, Hz
λ: Tire's side slip angle, degree
τ: The angular acceleration of wheels
ρ: Phase lag angle, degree
σ: Camber angle, degree.

Data Availability

The data used to support the findings of this study are included within the article.

Conflicts of Interest

The authors declare that there are no conflicts of interest regarding the publication of this paper.

Acknowledgments

This project was supported by National Natural Science Foundation of China (NSFC) (No. 51965026), Yunnan Province Applied Basic Research Foundation (No. 2018FB097), and the Scientific Research Fund Project of the Yunnan Provincial Education Department (No. 2018JS022). The authors are greatly appreciated for the financial support.

References

[1] M. Kazemi, K. Heydari Shirazi, and A. Ghanbarzadeh, "Optimization of semi-trailing arm suspension for improving handling and stability of passenger car," *Proceedings of the Institution of Mechanical Engineers, Part K: Journal of Multi-Body Dynamics*, vol. 226, no. 2, pp. 108–121, 2012.

[2] G. Mastinu, M. Gobbi, L. Yang, K. Ramakrishnan, and F. Ballo, "Suspension systems: some new analytical formulas for describing the dynamic behavior," SAE Technical Paper 2018-01-0554, SAE, Warrendale, PA, USA, 2018.

[3] S. Steišūnas, J. Dižo, G. Bureika, and V. Žuraulis, "Examination of vertical dynamics of passenger car with wheel flat considering suspension parameters," *Procedia Engineering*, vol. 187, pp. 235–241, 2017.

[4] W. Abbas, A. Emam, S. Badran, M. Shebl, and O. Abouelatta, "Optimal seat and suspension design for a half-car with driver model using genetic algorithm," *Intelligent Control and Automation*, vol. 4, no. 2, pp. 199–205, 2013.

[5] J. H. Crews, M. G. Mattson, and G. D. Buckner, "Multi-objective control optimization for semi-active vehicle suspensions," *Journal of Sound and Vibration*, vol. 330, no. 23, pp. 5502–5516, 2011.

[6] G. Šagi, Z. Lulić, and P. Ilinčić, "Multi-objective optimization model in the vehicle suspension system development process," *Tehnički Vjesnik*, vol. 22, no. 4, pp. 1021–1028, 2015.

[7] I. Javanshir, A. Maseleno, S. Tasoujian, and M. Oveisi, "Optimization of suspension system of heavy off-road vehicle for stability enhancement using integrated anti-roll bar and coiling spring mechanism," *Journal of Central South University*, vol. 25, no. 9, pp. 2289–2298, 2018.

[8] G. G. Fossati, L. F. F. Miguel, and W. J. P. Casas, "Multi-objective optimization of the suspension system parameters of a full vehicle model," *Optimization and Engineering*, vol. 20, no. 1, pp. 151–177, 2019.

[9] M. Gobbi, P. Guarneri, L. Scala, and L. Scotti, "A local approximation based multi-objective optimization algorithm with applications," *Optimization and Engineering*, vol. 15, no. 3, pp. 619–641, 2014.

[10] B. Gadhvi, V. Savsani, and V. Patel, "Multi-objective optimization of vehicle passive suspension system using NSGA-II, SPEA2 and PESA-II," *Procedia Technology*, vol. 23, pp. 361–368, 2016.

[11] Z. Zhao, B. Liu, C. Zhang, and H. Liu, "An improved adaptive NSGA-II with multi-population algorithm," *Applied Intelligence*, vol. 49, no. 2, pp. 569–580, 2019.

[12] B. J. Shi, D. H. Liu, and Z. Y. Li, "Parameterized analysis and optimization of vehicle anti-roll bar," *Journal of South China University of Technology*, vol. 44, no. 6, pp. 98–104, 2016.

[13] A. H. Joshi and H. S. Chhabra, "Mathematical model to find piercing point in McPherson strut suspension and design of profile for side force control spring," SAE, Warrendale, PA, USA, SAE Technical Paper 2012-28-0014, 2012.

[14] Ł. Konieczny, R. Burdzik, and P. Folęga, "Multibody system software used for research of car suspension system dynamics," *Advanced Materials Research*, vol. 1036, pp. 794–799, 2014.

[15] P. A. Simionescu and D. Beale, "Synthesis and analysis of the five-link rear suspension system used in automobiles," *Mechanism and Machine Theory*, vol. 37, no. 9, pp. 815–832, 2002.

[16] J. J. Zhu, A. Khajepour, E. Esmailzadeh, and A. Kasaiezadeh, "Overview introduction of vehicle dynamics with novel planar suspension systems," SAE, Warrendale, PA, USA, SAE Technical Paper 2011-01-0957, 2011.

[17] A. H. Tang, J. P. Tian, and X. X. Liu, "Kinematics characteristic analysis and structural parameter optimization of twist beam rear suspension," *Advanced Materials Research*, vol. 201–203, pp. 1710–1713, 2011.

[18] J. K. Martin and D. W. Parkins, "Notes on a simplified two-degree-of-freedom car suspension model of chassis heave and pitch-plane dynamics," *Proceedings of the Institution of Mechanical Engineers, Part K: Journal of Multi-Body Dynamics*, vol. 225, no. 3, pp. 252–262, 2011.

[19] M. Kazemi and K. H. Shirazi, "Handling enhancement of a sliding-mode control assisted four-wheel steer vehicle," *Proceedings of the Institution of Mechanical Engineers, Part D: Journal of Automobile Engineering*, vol. 226, no. 2, pp. 234–246, 2011.

[20] W. Lu, X. N. Gang, S. C. Zhi, B. J. Han, and C. Y. Wan, "Multi-objective bionics design method of passive suspension parameters based on hybrid behavior game," *Structural and Multidisciplinary Optimization*, vol. 42, no. 3, pp. 371–386, 2010.

[21] M. N. Khajavi, B. Notghi, and G. Paygane, "A multi objective optimization approach to optimize vehicle ride and handling characteristics," *World Academy of Science, Engineering and Technology*, vol. 38, pp. 580–584, 2010.

[22] G. Georgiou, G. Verros, and S. Natsiavas, "Multi-objective optimization of quarter-car models with a passive or semi-active suspension system," *Vehicle System Dynamics*, vol. 45, no. 1, pp. 77–92, 2007.